Journal of Hydrology: Regional Studies 50 (2023) 101563

Contents lists available at ScienceDirect

Journal of Hydrology: Regional Studies

journal homepage: www.elsevier.com/locate/ejrh

Improved modeling of Congo's hydrology for floods and droughts analysis and ENSO teleconnections

Sly Wongchuig [a,*], Benjamin Kitambo [a,b,c], Fabrice Papa [a,d], Adrien Paris [a,e], Ayan Santos Fleischmann [f], Laetitia Gal [a,e], Julien Boucharel [a,g], Rodrigo Paiva [h], Rômulo Jucá Oliveira [a], Raphael M. Tshimanga [b], Stéphane Calmant [a]

[a] Laboratoire d'Etudes en Géophysique et Océanographie Spatiales (LEGOS), Université de Toulouse, CNES/CNRS/IRD/UT3, Toulouse, France
[b] Congo Basin Water Resources Research Center (CRREBaC) & the Regional School of Water, University of Kinshasa (UNIKIN), Kinshasa, Democratic Republic of the Congo
[c] Faculty of Sciences, Department of Geology, University of Lubumbashi (UNILU), Route Kasapa, Lubumbashi, Democratic Republic of the Congo
[d] Institute of Geosciences, Campus Universitario Darcy Ribeiro, Universidade de Brasília (UnB), 70910-900 Brasilia, DF, Brazil
[e] Hydro Matters, 1 Chemin de la Pousaraque, 31460 Le Faget, France
[f] Instituto de Desenvolvimento Sustentável Mamirauá, Tefé, AM, Brazil
[g] Department of Atmospheric Sciences, School of Ocean and Earth Science and Technology (SOEST), University of Hawai'i at Mānoa, 2525 Correa Road, Honolulu, HI 96822, USA
[h] Instituto de Pesquisas Hidráulicas IPH, Universidade Federal do Rio Grande do Sul UFRGS, Brazil

ARTICLE INFO

Keywords:
Hydrological reanalysis
Hydrological-hydrodynamic modeling
Lakes storage
Dynamics
Data assimilation
Congo River basin
Hydrological extreme events

ABSTRACT

Study region: The Congo River basin (CRB), the world's second-largest river system, is subject to extreme hydrological events that strongly impact its ecosystems and population.
Study focus: Here we present an improved 40-year (1981–2020) hydrological reanalysis of daily CRB discharge and analyze the spatiotemporal dynamics of recent major CRB floods and droughts, and their teleconnection with El Niño-Southern Oscillation (ENSO), the dominant driver of tropical precipitation. We employ a large-scale hydrologic-hydrodynamic model (MGB) with lake storage dynamics representation and a data assimilation (DA) technique using in-situ and remote sensing observations.
New Hydrological Insights: The MGB model demonstrates satisfactory performance, with Kling-Gupta efficiency metric of 0.84 and 0.71 for calibration and validation, respectively. Incorporating lake representation substantially enhances simulations, increasing the Pearson correlation coefficient from 0.3 to 0.63. Additionally, DA yields a ~13% reduction in discharge errors via cross-validation. We find that the 1997–1998 flood impacting the south and central CRB is statistically linked to a major El Niño event during that period. However, no such association is found for the 2019–2020 flood. Severe droughts in 1983–1984 and 2011–2012, affecting northern and southern CRB respectively, exhibit strong correlation with preceding El Niño and La Niña events, with a ~10–12 months lag. This study advances understanding of the intricate interplay between spatiotemporal hydrological variability in CRB and large-scale climate phenomena like ENSO.

* Corresponding author.
E-mail address: sly.wongchuig-correa@univ-tlse3.fr (S. Wongchuig).

https://doi.org/10.1016/j.ejrh.2023.101563
Received 10 July 2023; Received in revised form 30 October 2023; Accepted 1 November 2023
Available online 3 November 2023

1. Introduction

The Congo River basin (CRB) is the second-largest basin in the world both in terms of drainage area and discharge to the ocean with a mean annual flow rate of 40,500 $m^3 s^{-1}$ at Kinshasa/Brazzaville (Beighley et al., 2011; Laraque et al., 2020). The CRB with its vast and complex hydrological system is also home to the world's second-largest rainforest, which is one of the most climate sensitive regions on the planet (Zelazowski et al., 2011), especially regarding the potential impacts of climate change (James et al., 2013; Vizy and Cook, 2012). However, the CRB remains largely understudied, poorly monitored (Nicholson et al., 1988; Washington et al., 2013) and has not received adequate attention in terms of hydrological and climate research (Alsdorf et al., 2016; Tshimanga and Hughes, 2014; Washington et al., 2006). These conditions limit the understanding of the processes that control Congo's hydrology dynamics in a spatially and temporally coherent manner and prevent the development of appropriate and sustainable water resources management strategies in the CRB.

The CRB has been subject to extreme hydrological events such as droughts and floods which have affected more than 10 million people living in the nine countries covered by the CRB. Several studies have highlighted the vulnerability of the CRB to these extreme hydrological events, including the recent 2020 flood (Bola et al., 2022; Mugisho Bachinyaga et al., 2022; "Republic of Congo," 2020), and the 1998, 2005–2006 and 2016–2017 droughts (Ndehedehe et al., 2019; Sorí et al., 2022). Other studies have examined the climatic variability and trends in the region over relatively longer time periods (Ayugi et al., 2022; Chambers and Roberts, 2014; Mabrouk et al., 2022; Masih et al., 2014; Zhou et al., 2014), as well as the impact of precipitation patterns on hydrological variability (Ndehedehe and Agutu, 2022). In general, it has been shown that extreme events in the CRB are mainly related to i) rainfall and evapotranspiration variability, which may have been exacerbated by climate change in recent decades and to ii) changes in the hydrological response of the basin, for example due to anthropogenic disturbances for instance (Gosset et al., 2023; Karam et al., 2022). By studying hydroclimatic variability and extreme events in the CRB, we can gain critical insights into the region's vulnerability to climate change and identify effective strategies for sustainable development and climate resilience.

On the other hand, many hydrological models capable of representing the dynamics of the large-scale water cycle have been developed in recent years (Paiva et al., 2011; Singh, 2018; Yamazaki et al., 2012), which could help to overcome the lack of in-situ observations in the CRB (Kitambo et al., 2022). Up to now, the application of hydrological modeling in the CRB has been evaluated mainly to understand the hydrological variability in space and time and the dominant processes on a regional to large scales, by using different types of models, statistical, and process-based hydrologic and hydrodynamic models (Datok et al., 2022; Dos Santos et al., 2022; O'Loughlin et al., 2019; Paris et al., 2022; Tshimanga et al., 2022, 2011). Beyond the scarcity of hydrological data, these modeling framework have been challenged by other many issues, including its geographic extent, the natural complexity of the processes to be modeled (Munzimi et al., 2019; Paris et al., 2022), the understanding of the processes (Kabuya et al., 2022; Tshimanga et al., 2022), and the uncertainty of the model structures and parameters (Tshimanga et al., 2011). Other challenges are related to the integration of natural storage modeling of lakes and wetlands, which dominate the basin hydrology, into the model structure (Paris et al., 2022; Tshimanga and Hughes, 2014), especially along the Cuvette Centrale (Paris et al., 2022).

In addition to modeling, some techniques such as data assimilation (DA) have been developed in the last decades to update model state variables by optimally combining model simulation and observations (Liu et al., 2016; Sun et al., 2016). Their application in large-scale hydrology has had different objectives such as the study of past extreme events (Wongchuig et al., 2019) and streamflow forecasting (Andreadis et al., 2017; Paiva et al., 2013). To our knowledge, only in recent years few studies such as (Revel et al., 2019) and (Apers et al., 2023) have used DA in hydrologic models in the CRB. The first one used DA as a proof of concept to test a localization methodology and not to generate actual and long-term streamflow series, while the second one, only to simulate and study a specific region of the Congo peatlands in the Cuvette Centrale.

In this context, here we present the improvement of a semi-distributed, large-scale hydrological-hydrodynamic model (Collischonn et al., 2007; Paris et al., 2022) by integrating for the CRB, i) the representation of lakes storage dynamics and ii) the assimilation of in-situ discharge and water level series to yield long-term hydrological variables. Additionally, the largest amount of existing in-situ data from the region has been used for the calibration, validation and assimilation process during the last 40 years. The main objective is to improve current estimates of river discharges in a spatially distributed manner throughout the CRB, in order to identify and study extreme events over the last 40 years as well as their potential hydroclimatic triggers and large-scale teleconnections. Considering that many studies are mainly focused only on the variability in precipitation (Diem et al., 2021; Mabrouk et al., 2022), in part because of considerable lack of in-situ discharge observations.

Section 2 describes briefly the study area, datasets used, model set-up and experiment design. Section 3 provides the results of the calibration and validation, and the final long-term simulation. We discussed analysis of particular hydrological extreme events and possible links to large-scale climate variability, especially related to the El Niño-Southern Oscillation (ENSO), which drives larger year to year variations in ocean temperature in the tropical Pacific. ENSO is also considered the largest driver of tropical precipitation on interannual timescales and with significant influences on the sea surface temperature (SST) in other tropical oceans (Bhavani et al., 2017; Yuan et al., 2012). In that sense, supplementary analyses were also discussed considering Tropical Indian Ocean (TIO) indices such as the TIO SST anomalies and the Indian Ocean Dipole Mode Index (DMI).

2. Material and methods

2.1. Study area

The CRB is located in central Africa astride the equator, with many characteristics of a tropical humid ecosystem. The CRB spans

over nine riparian countries including Central African Republic, Cameroon, Republic of the Congo, Angola, Democratic Republic of Congo (DRC), Zambia, Tanzania, Rwanda, and Burundi (Fig. 1). Of these riparian countries, the DRC also holds ~70% of the drainage area. In addition to a dense hydrographic network of the basin, there are also many wetlands and lakes of global significance. Some of the major lakes of the CRB encompass the Tanganyika, Kivu, Tumba, Mai-Ndombe, Bangweulu, Mweru, and Zimbambo.

The annual rainfall is ~1900 mm yr^{-1} along an east-west trend across the basin, decreasing northward and southward to ~1100 mm yr^{-1} (Alsdorf et al., 2016). The rainfall seasonality also varies in space, which is mainly modulated due to the bi-annual passage of the inter-tropical convergence zone (ITCZ) across the basin. The quality (migration/stationarity) of the ITCZ together with the influence of teleconnection patterns, such as the ENSO, has a direct impact on the spatio-temporal organization of convection and, consequently, on the distribution of precipitation over the region (Nicholson, 2018). Thus, distinct mechanisms, such as dynamics (e.g. ITCZ, ENSO) and local and mesoscale thermodynamics (Nicholson et al., 2022), in addition to surface characteristics, are key to understanding the extreme hydrological events that are intrinsically associated with the occurrence of extreme weather and climate episodes over the region.

The Mbandaka and Brazzaville regions, located in the central part of the basin, have a less marked seasonality. The northern region has their wettest period during March to May, while the southern region shows regular double-peak cycles (bimodality) with the highest water levels in November-December and March-April (Kelemen et al., 2021; Paris et al., 2022; Samba et al., 2008) (Fig. S1).

2.2. The MGB hydrologic-hydrodynamic model

The MGB (Portuguese acronym for Large Basins Model) is a semi-distributed, large-scale hydrological model that uses physical and conceptual equations to simulate land surface hydrological and hydrodynamic processes (Collischonn et al., 2007; de Paiva et al., 2013; Siqueira et al., 2018). The model discretizes the basin into unit-catchments and uses the hydrological response units (HRUs) approach, which combines soil type and land use within each unit. The simulated vertical hydrological processes in MGB are calculated based on the variable contributing area concept. This means that for each HRU of each unit-catchment, the model simulates the soil water budget using a bucket model, the energy budget and evapotranspiration, interception, soil infiltration, runoff and also the generation of subsurface and groundwater flow (Fig. 2).

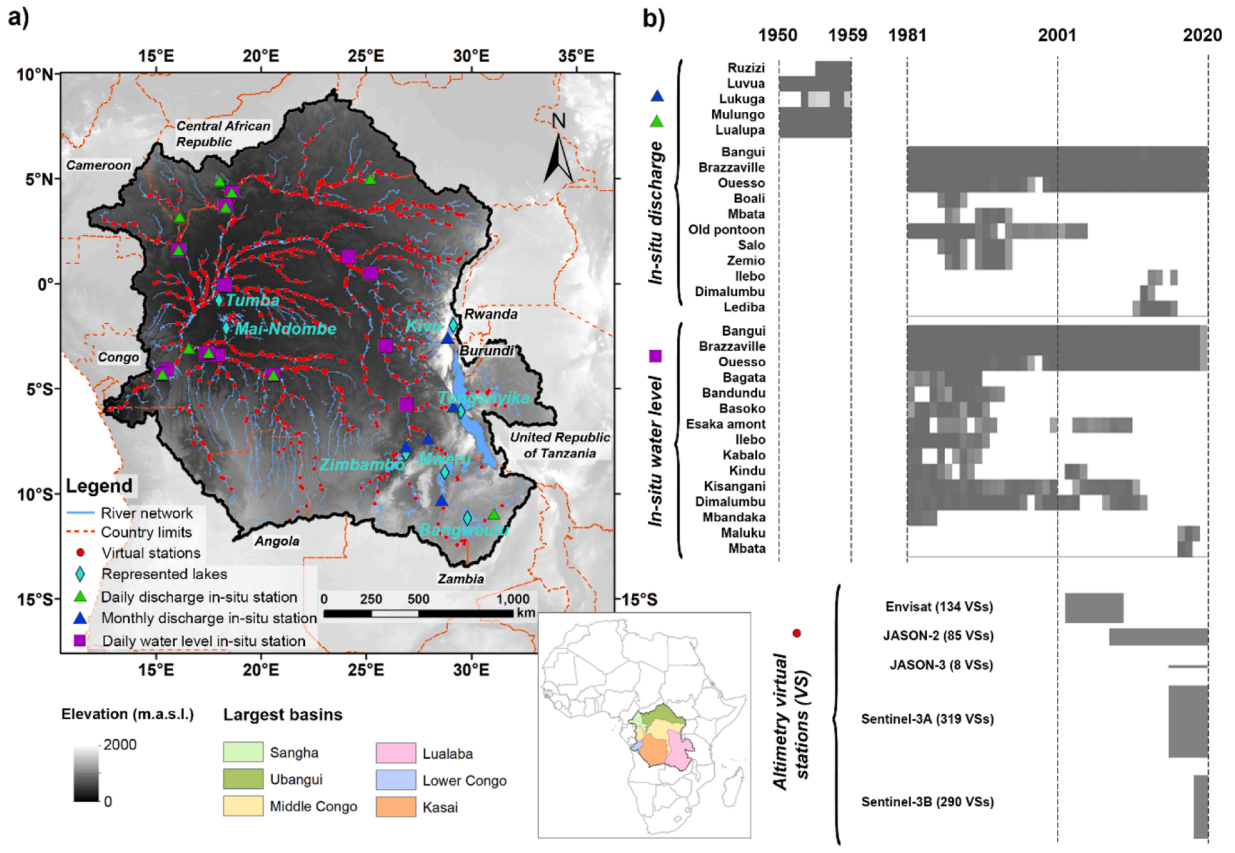

Fig. 1. (a) Map of the Congo River basin, its terrain elevation and country boundaries. The in-situ stations for discharge (triangles), water level (squares), satellite altimetry derived water levels (circles), and the seven lakes (diamonds) represented in this study's model are overlaid on the map. (b) Temporal availability of observed discharge and water level from in-situ stations, as well as water level virtual stations from radar altimetry, for the period 1950–2020.

The propagated discharge in the main network of each unit-catchment is the sum of the flow from the upstream drainage area and the flow generated in the unit-catchment itself. Flow routing is computed using the local inertial method (Pontes et al., 2017), which is a simplification of the 1D Saint-Venant equations in which the advective inertial term is neglected (Bates et al., 2010; Pontes et al., 2017).

The lake routing and data assimilation modules implementation in the MGB model are described in Sections 2.4.1 and 2.4.2, respectively. More detailed information for the MGB hydrologic-hydrodynamics components and equationing can be found in the Supplementary material, in (Collischonn et al., 2007) and in (Pontes et al., 2017).

2.3. Datasets

2.3.1. Model forcing

The Climate Hazards Group InfraRed Precipitation with Station (CHIRPS) precipitation dataset (Funk et al., 2015), as well as ERA5 reanalysis (Copernicus Climate Change Service, 2019) information for atmospheric air pressure, radiation fluxes, wind speed, relative humidity and surface air temperature were used to force the MGB model.

CHIRPS is based on precipitation models that are merged with in-situ precipitation data (Funk et al., 2015). The latest version CHIRPS v2.0 was used in this study with a spatial resolution of 0.05° x 0.05° on a daily time scale. Precipitation data for each unit-catchment are obtained by the interpolation to each CHIRPS pixel, using the nearest neighbor algorithm. (Dos Santos et al., 2022) and (Kouakou et al., 2023) reported a satisfactory performance of CHIRPS v2.0 throughout the CRB and in its northern region, respectively, when evaluated against other satellite-based precipitation datasets in a large-scale hydrologic model.

Climate variables used to compute evapotranspiration were retrieved from ERA5 which is a global atmospheric reanalysis dataset from the European Centre for Medium-Range Weather Forecasts (ECMWF) that provide a large number of atmospheric, land, oceanic and climate variables at a spatial resolution of ~30 km and from a temporal resolution of 1-hourly time step spanning the period 1950 to present (Copernicus Climate Change Service, 2019; Tarek et al., 2020). In the MGB, we consider the long-term monthly climatology of the ERA5 reanalysis variables that is applied internally in the calculations for each day (corresponding to each month) for each unit-catchment. Finally, the outputs of the state variables of the MGB model are at daily time steps.

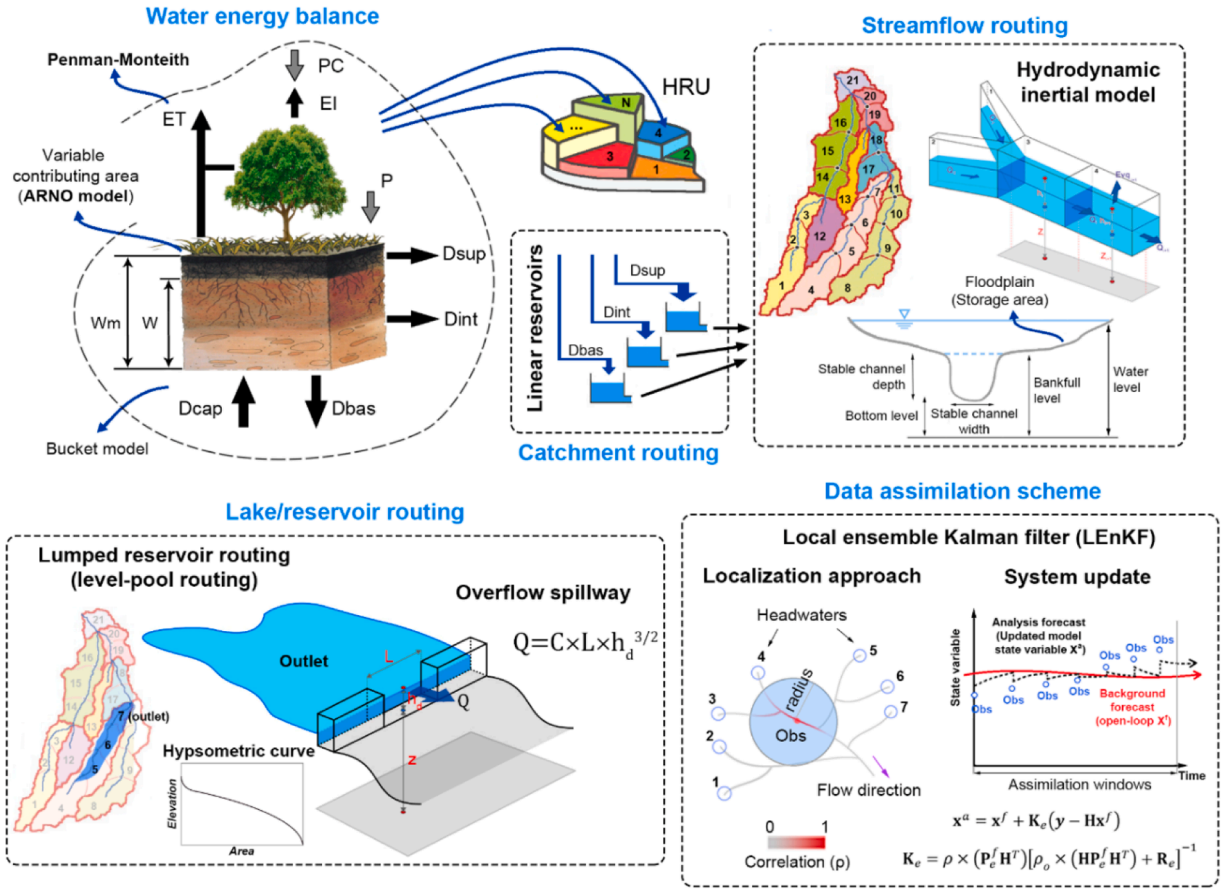

Fig. 2. Schematic of the general structure of the MGB hydrologic-hydrodynamic model.

2.3.2. Observations for model calibration, validation and assimilation

Here we used a consolidated database of: (i) in-situ stations (i.e., 12 of discharge and 15 of water level from 1981 to 2020) acquired from the Congo Basin Water Resources Research Center (CRREBaC, <https://www.crrebac.org/>, last access: August 2022), the Environmental Observation and Research project (SO-HyBam, <https://hybam.obs-mip.fr/fr/>, last access: September 2022), and from the Global Runoff Data Centre database (GRDC, <https://www.bafg.de/GRDC/EN/02_srvcs/21_tmsrs/210_prtl/prtl_node.html>, last access: September 2022); (ii) radar altimetry-derived water level dataset (i.e., a total of 836 virtual stations (VSs) over the period 1995–2020) for calibration, validation and assimilation and (iii) water level data for lakes obtained by radar altimetry (five VSs for lakes over the period 2001–2020). (ii) and (iii) were obtained from the Theia Hydroweb database (available at: <https://hydroweb.theia-land.fr/>, last access: October 2022). Consider that the VSs do not have a fixed temporal resolution among the different altimetry radar sensors (Jason, Envisat and Sentinel), which can vary from 9.9 to 35 days. More details about these datasets can be found in (Kitambo et al., 2022).

Due to the variable temporal availability of the data for each station, only seven in-situ daily discharge and nine daily water level gauges (Table 1 and Fig. 1 for their locations) were used to calibrate MGB during the set-up phase, which spans from 01/01/2001–31/12/2020. In addition to these contemporary observations overlapping the set-up period, the oldest observations from eight daily discharge and 13 daily water level stations from 1981 were used to validate MGB (see temporal availability in Fig. 1b). For the calibration of the lake's parameters, historical discharge data were used from five stations on a monthly time scale from 1950 to 1959 (from historical stations, i.e, in situ observations before the 1990 s, Table 1). Considering the period of the hydrological modeling set-up, the calibration of the lakes' dynamics was performed by analyzing the monthly climatology of the series and the validation was performed by using lakes VSs during the recent period (2001–2020).

Our criterion for choosing the calibration period has been mainly to give priority to the general availability of data from either discharge, in-situ water level or VSs, then to the availability of observed discharge data which was relevant for calibration of the lakes' dynamics.

2.4. Model set-up

The model pre-processing, which includes the generation of the drainage network using a digital elevation model and the generation of the hydrologic response units using land use maps, is described in detail in the Supplementary material.

2.4.1. Lake routing

The Congo basin hydrology contains several lakes and wetlands which play an important role in the hydrological regime of the basin through their capacity to store water, leading to flow attenuation and regulation, delays and increased residence time (Tourian

Table 1
Summary of in-situ discharge and water level stations for model calibration and validation.

ID	Station name	Lat	Lon	Data	Temporal resolution *	Use for **	Period
1	Bangui	4.37	18.61	Discharge/ Water level	D	Cal-Val / Cal-Val	1981–2020
2	Brazzaville	-4.30	15.30	Discharge/ Water level	D	Cal-Val / Cal-Val	1981–2020
3	Ouesso	1.62	16.065	Discharge/ Water level	D	Cal-Val / Cal-Val	1981–2020
4	Boali	4.905	18.025	Discharge	D	Val	1985–1988
5	Mbata	3.663	18.302	Discharge	D	Val	1986–1994
6	Old Pontoon	-10.95	31.07	Discharge	D	Cal-Val	1981–2004
7	Salo	3.201	16.122	Discharge	D	Val	1985–1994
8	Zemio	5.002	25.195	Discharge	D	Val	1986–1994
9	Ilebo	-4.33	20.58	Discharge/ Water level	D	Cal / Val	2013–2016 / 1981–1991
10	Dimalumbu	-3.275	17.498	Discharge/ Water level	D	Cal / Cal-Val	2012–2013 / 1981–2012
11	Lediba	-3.057	16.557	Discharge	D	Cal	2011–2016
12	Bagata	-3.39	17.4	Water level	D	Val	1981–1990
13	Bandundu	-3.3	17.37	Water level	D	Val	1981–1993
14	Basoko	1.28	24.14	Water level	D	Val	1981–1991
15	Esaka amont	-3.402	17.944	Water level	D	Cal-Val	1981–2010
16	Kabalo	-5.74	26.91	Water level	D	Val	1981–1990
17	Kindu	-2.95	25.926	Water level	D	Cal-Val	1981–2004
18	Kisangani	0.51	25.19	Water level	D	Cal-Val	1981–2011
19	Mbandaka	-0.07	18.26	Water level	D	Val	1981–1984
20	Maluku	-4.07	15.51	Water level	D	Cal	2017–2019
21	Mbata	3.663	18.302	Water level	D	Cal	2017–2018
Stations with historical data							
1	Lualupa	-10,36	-10,36	Discharge	M	Cal Lake Bangweulu	1950–1959
2	Lukuga	28,62	28,62	Discharge	M	Cal Lake Tanganyika	1952–1959
3	Luvua	-5,91	-5,91	Discharge	M	Cal Lake Mweru	1950–1959
4	Mulungo	29,19	29,19	Discharge	M	Cal Lake Zimzambo	1950–1959
5	Ruzizi	-7,34	-7,34	Discharge	M	Cal Lake Kivu	1955–1959

* D=Daily, M=Monthly
** Cal=Calibration, Val=Validation

et al., 2023; Tshimanga et al., 2022). In the first version of the MGB model developed for the CRB by (Paris et al., 2022), the lake hydrological processes were not taken into account. Here, the hydrological functions of seven lakes were considered, including Bangweulu, Mweru, Tanganyika, Kivu, Zimbambo, Tumba, and Mai-Ndombe Lakes (Fig. 1). In order to properly represent the hydrology of the basin, a lake routing scheme was implemented, based on (Fleischmann et al., 2019, 2021) and based on a lumped (level-pool) approach. This computes a simple and lumped continuity equation for a given lake assuming a horizontal water level, represented here by the unit-catchment identified as the outlet of each lake (see Fig. 2).

The variation of storage within the lake area is computed by the continuity equation (Eq. s2) already defined in the hydrodynamic routing method in MGB. The storage is adjusted by replacing the respective unit-catchments' level–storage relationship by the one representative of the lake. For this purpose, a pre-processing was developed in each lake's outlet in which a representative level-

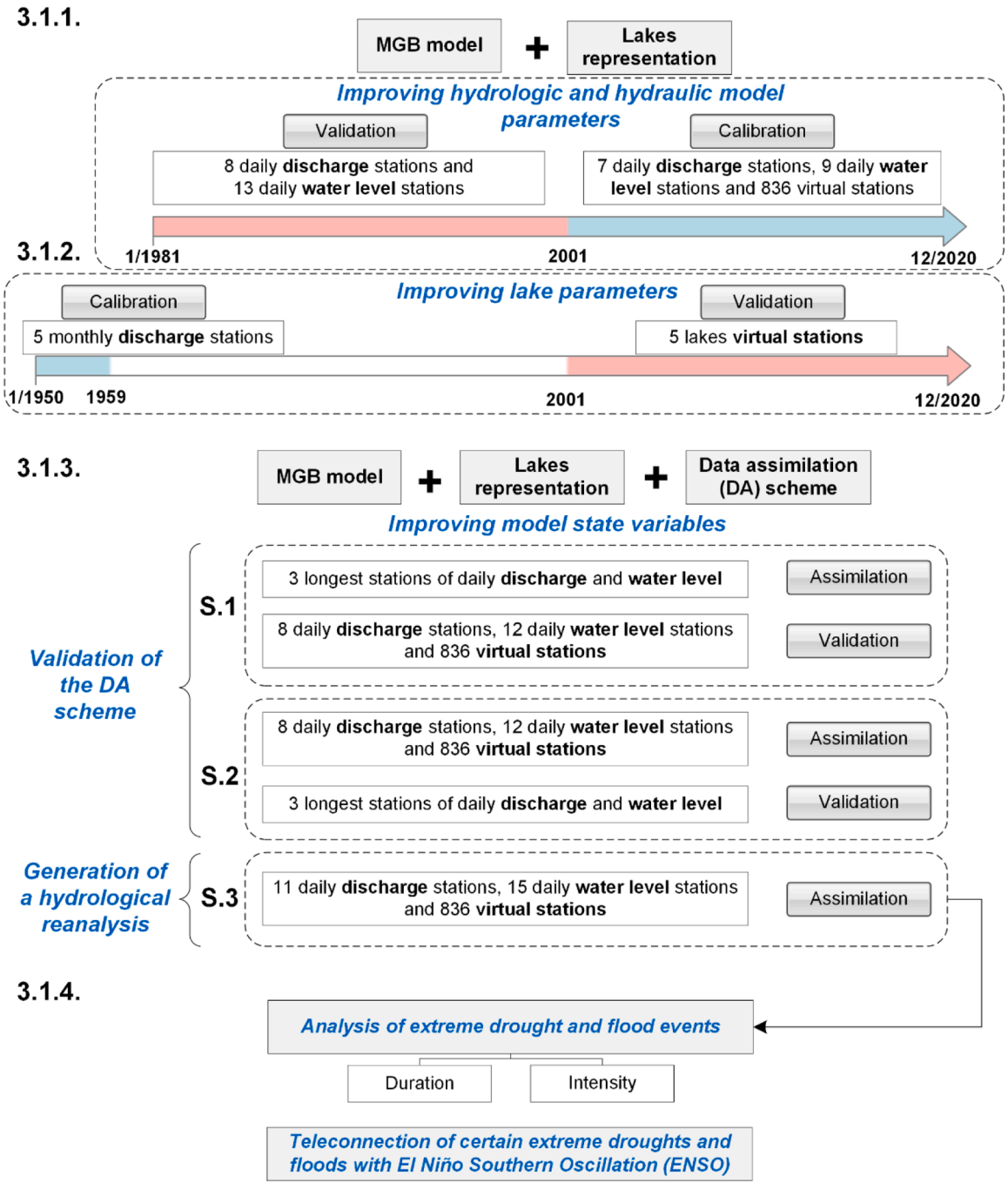

Fig. 3. Schematic representation of the experiment set-up divided by the manuscript's sections.

storage relationship was defined by using satellite altimetry and flooded area from the Theia Hydroweb database.

The second characteristic that defines the simulation of a lake is its outflow equation, defined here as a rectangular spillway structure, represented as an internal boundary condition, and defined as follows:

$$Q = C \bullet L \bullet h_d^{\frac{3}{2}} \quad (1)$$

where Q is the spillway outflow, C the spillway discharge coefficient, L the spillway length and h_d represents the water depth above the crest of the spillway level.

The C parameter was adjusted during calibration for each lake, while L was estimated as the lake width at the lake's outlet, based on high-resolution Google satellite imagery acquired in February 2023.

2.4.2. Data assimilation approach

Among the data assimilation (DA) methods that have been implemented in the field of hydrology, the ensemble Kalman filter (EnKF) has become popular because it allows a simplified implementation in hydrological models in which non-linear processes predominate (Moradkhani, 2008; Wongchuig et al., 2019). This method uses an ensemble of state variables to sample the model errors and compute the covariance error matrix, which is used to estimate the Kalman gain. For this purpose, it is common to estimate these errors from the perturbation of the model forcing or parameters (Biancamaria et al., 2011; Liu et al., 2012; Paiva et al., 2013). Among the EnKF-based methods, the local ensemble Kalman filter (LEnKF) was adopted in this study, which was implemented and evaluated in MGB (Wongchuig et al., 2020b, 2019).

This localization method proposed by (Houtekamer and Mitchell, 2001) and implemented here limits the update of the state variable to a spatial range from the observation. The radius of influence has been evaluated in previous works for large basins such as the Amazon (Emery et al., 2018; Wongchuig et al., 2019), leading to optimal values from 500 to 2000 km. In the present work we choose 2000 km, so that the assimilation improvements spread over at least 43% of the area with a correlation greater than 0.5 (see Fig. S4), even when only three stations are assimilated in the whole basin. For more details on the equationing, implementation and performance of the LEnKF scheme in MGB see the Supplementary material and (Wongchuig et al., 2020b, 2020a, p. 2, 2019).

2.5. Experimental design

2.5.1. Calibration and validation

The objective of this section is to show the experimental process to obtain the satisfactory hydrologic and hydraulic parameters of the MGB based on the statistical metrics shown in Section 2.5.4. Fig. 3 presents a complete schematic representation of our experimental design. The MGB model was set-up at the daily time scale over two periods. The first one over the period 01 January 2001–31 December 2020 for calibration and the second one over the period 01 January 1981–31 December 2000 for validation. For this we use in-situ daily discharge and daily water level series as well as satellite altimetry from VSs (see Section 2.3.2 and Table 1). Only during the validation phase no satellite feed data were used due to the non-consistent data during this period. The in-situ stations present daily data and the VSs from altimetry range between 9.9 and 35 days. These periods of calibration and validation were chosen also to take advantage of the satellite-derived water level over the recent period to calibrate the MGB hydraulic parameters. A spin-up period of two years was selected to eliminate the influence of initial conditions. The parameters to be calibrated within the MGB are mainly divided into hydrological and hydraulic. The hydrologic parameters (see Table S1) are mainly associated with soil conditions in the runoff generation process. As for the hydraulic parameters, they are associated with the hydraulic geometry which are the stable width and depth of the main river channel for each unit-catchment.

For the calibration of the lake's parameters of the MGB, five stations with historical series of monthly discharge during the period 1950–1959 were used, which are located downstream of their associated lakes (see Table 1). The lake parameters are mainly hydraulic (see Section 2.4.1) such as C the spillway discharge coefficient, L the length of the spillway and h_d which represents the depth of water above the crest of the spillway level. The validation of the series was performed by comparing the water level anomalies between the simulations at each lake outlet with information from VSs developed specifically for each lake in the Theia database for the period 2001–2020.

2.5.2. Data assimilation

Secondly, we performed a long-term simulation from 1981 to 2020 with the LEnKF DA approach. The objective of this second part is to improve the state variables of the model along the whole basin. At this stage, three major experiments were performed (Fig. 3), two of which were for validation purposes. These experiments were: (S.1) Assimilation of the discharge and water level anomaly of the three stations with most continuous and longest availability in the basin (Bangui, Brazzaville and Ouesso), and validation with all the remaining stations; (S.2) Assimilation of the discharge and water level anomaly of the stations with less data and validation with the three stations with more continuous and longest data; (S.3) Assimilation of all the available in-situ and radar altimetry information. After a proper validation, we were able to use MGB to improve our understanding of the basin's interannual and seasonal water variability, and identify major hydrological extreme events (i.e. 1983–1984 droughts and 1997–1998 or 2019–2020 floods).

2.5.3. Extreme events analysis considering duration and intensity

In this section we analyzed the discharge time series from the observations and simulations, which were deseasonalized using a multiplicative method. When using this method, daily discharges belonging to a given month are multiplied by the ratio between the

monthly climatology and the annual or historical climatology of the discharge (see Eq. 2). In this way, orders of magnitude similar to the original series are maintained and negative values are avoided.

$$Q_{des,d} = Q_{non-des,d} \bullet \frac{\left(\overline{Q_{non-des,d}}\right)_m}{\left(\overline{Q_{non-des}}\right)_{yr}} \quad (2)$$

where $Q_{des,d}$ is the daily deseasonalized discharge, calculated by the product of $Q_{non-des,d}$ which is the daily non-deseasonalized discharge and the ratio between $\left(\overline{Q_{non-des,d}}\right)_m$ which corresponds to the monthly climatology to which the analyzed day belongs and the $\left(\overline{Q_{non-des}}\right)_{yr}$ which is the annual or historical climatology of the discharge during the total period (1981–2020).

Thus, for the duration analysis we used a simple concept to consider the number of days above or below a certain threshold (Marengo et al., 2013; Tabari, 2021; Wongchuig et al., 2017). This threshold was defined as half of the standard deviation of the annual maximum and minimum events, after testing a range from 0.5 to 1 of the standard deviation. We used this value because it represents in a spatially continuous manner different extreme hydrologic events in the drainage network that have been documented in the literature. For the intensity we based our analysis on the return period analysis by considering the extreme value theory (EVT) (Faragó and Katz, 1990; Katz et al., 2002) with a Peak Over threshold (POT) method (Marengo et al., 2013; Nadarajah and Shiau, 2005). To estimate the return period, we use the Generalized Pareto Distribution (GPD) (Balkema and de Haan, 1974; Hosking and Wallis, 1987; Pickands, 1975) which is a probability distribution function used to model the tails of a distribution. GPD is often used to model the distribution of exceedances above a certain threshold, and is therefore also used to estimate the probability of extreme events in hydrology, such as floods and droughts (e.g. Anghel and Ilinca, 2023; Zhou et al., 2017).

To assess potential relationships between extreme hydrological events in the CRB and the large-scale climate patterns associated with ENSO during the period 1981–2020, we have used the classic Niño-3.4 SST index calculated as the sea surface temperature (SST) interannual anomalies, i.e. SST cleared from their monthly mean climatology and averaged over the central Pacific region [5 N-5S 170–120 W] (available at: <https://psl.noaa.gov/gcos_wgsp/Timeseries/Nino34/>, last access on April 2023). El Niño (La Niña) events were then identified when values of the Niño-3.4 SST index were above (below) the standard deviation for at least six consecutive months, which is a variation of the standard methodology for identifying ENSO events (e.g., Trenberth, 1997). This value which is about 1 °C compared to the traditional value of 0.4 °C, allows the categorization of extreme El Niño and La Niña events. Specific extreme hydrological events were selected and it was identified whether they were associated with El Niño or La Niña events. In addition, composite maps are calculated for the normalized discharge anomaly during La Niña and El Niño periods. The lagged Pearson correlation coefficient maps showing the maximum value and the number of months of time lag between the discharge anomaly and the Niño-3.4 SST index are also calculated. The Pearson correlation coefficient has been associated to P-values below 0.05, then it can be considered statistically significant. Similar analyses were performed for two additional indexes in the Supplementary material, the Tropical Indian Ocean (TIO) SST anomalies and the Indian Ocean Dipole (IOD) considered as a dominant interannual phenomenon in the TIO (An, 2004; Huang et al., 2016; Webster et al., 1999). For the second one, the Indian Ocean Dipole Mode Index (DMI) has been used, defined as the difference in SST anomalies between the western TIO (50°E to 70°E and 10°S to 10°N; IODW) and the southeastern TIO (90°E to 110°E and 10°S to 0°S; IODE) (Saji et al., 1999). The procedure to determine the negative and positive phases of the TIO SST and the DMI index were similar to the methodology used to determine the extreme events of La Niña and El Niño for ENSO. For this purpose, the monthly SST from the ERA5 reanalysis was used (available at: <https://cds.climate.copernicus.eu/cdsapp#!/dataset/reanalysis-era5-single-levels-monthly-means>, last access on September 2023).

We use this exploratory analysis as numerous have demonstrated the importance of SST variations in explaining African precipitation variability studies (Folland et al., 1986; Hoerling et al., 2006), providing an entry point for reliable attribution studies of extreme hydrological events in the CRB.

Table 2
Efficiency metrics used in this study.

Metric	Assessment	Equation	
Pearson's correlation coefficient (r)	Linear correlation	$r = \frac{n\sum x_{sim}x_{obs} - (\sum x_{sim}\sum x_{obs})}{\sqrt{n\sum x_{sim}^2 - (\sum x_{sim})^2}\sqrt{n\sum x_{obs}^2 - (\sum x_{obs})^2}}$	(3)
Nash–Sutcliffe efficiency (NSE)	High flows	$NSE = 1 - \frac{\sum (x_{sim} - x_{obs})^2}{\sum (x_{obs} - \overline{x_{obs}})^2}$	(4)
Kling–Gupta efficiency (KGE)	Overall performance	$KGE = 1 - \sqrt{(r-1)^2 + \left(\frac{\sigma_{sim}/\mu_{sim}}{\sigma_{obs}/\mu_{obs}} - 1\right)^2 + \left(\frac{\mu_{sim}}{\mu_{obs}} - 1\right)^2}$	(5)
Relative bias (%)	Under- and overestimation (volume)	$\text{Relative bias}(\%) = \left(\frac{\sum x_{sim} - \sum x_{obs}}{\sum x_{obs}}\right) \times 100$	(6)
Difference in the relative root mean square error (ΔRRMSE)	Deviation of predicted values	$RRMSE = \sqrt{\frac{\sum \left(\frac{x_{sim} - x_{obs}}{x_{obs}}\right)^2}{n}}, \quad \Delta RRMSE = \frac{RRMSE_{assimilation} - RRMSE_{open-loop}}{RRMSE_{open-loop}}$	(7)

2.5.4. Metrics for assessment of results

A number of efficiency metrics were used to evaluate the model's performance during the calibration and validation phases. These include the Pearson correlation coefficient (r), Nash–Sutcliffe efficiency (NSE), Kling–Gupta efficiency (KGE), relative bias and differences in the relative root-mean-square error (ΔRRMSE). The NSE is a normalized statistic that determines the relative magnitude of residual variance compared with the observed data variance, while the KGE offers more general results in model performance, because it uses the most components, such as correlation, variability and bias terms. Both NSE and KGE range between $-\infty$ and 1 (perfect fit). The ΔRRMSE metric was used to compare relatively the open-loop (i.e. simulation without assimilation) with the run with assimilation, more negative values indicate a greater reduction of errors by the DA technique. The equations for each of the above metrics are provided below in Table 2:

where x_{sim} and x_{obs} are the simulated and observed variable, respectively, σ is the standard deviation and μ is the mean, n is the total number of observations.

3. Results and discussions

3.1. Model calibration and validation

3.1.1. In-situ river discharge and water level

Overall, the MGB model simulated very satisfactory daily discharges during the calibration step. The median values of KGE, NSE and relative bias were 0.84%, 0.73% and 1.7%, respectively (Fig. 4). The lowest values of NSE and KGE are observed at the most downstream gauge of Brazzaville. This can be attributed to the overestimation of water volume by the model at the second peak of the annual hydrograph, which is the result of the aggregation of different hydrological temporal patterns contributing to this particular point of the basin. The largest model overestimation is found around 2018–2019 at Brazzaville and Bangui stations, both in the time series and in the scatterplot panels on the right side of each series, because of an overestimation of the CHIRPS precipitation. Similarly, the water level performance is shown in Fig. S5, where the NSE and Pearson correlation coefficient show values of 0.52 and 0.82 respectively. A better performance occurs in the northern part of the CRB, which varies less on seasonal timescales than the southern one.

Fig. 5 shows the time series of water level anomaly and the spatial distribution of the statistical indices for 836 VSs during the

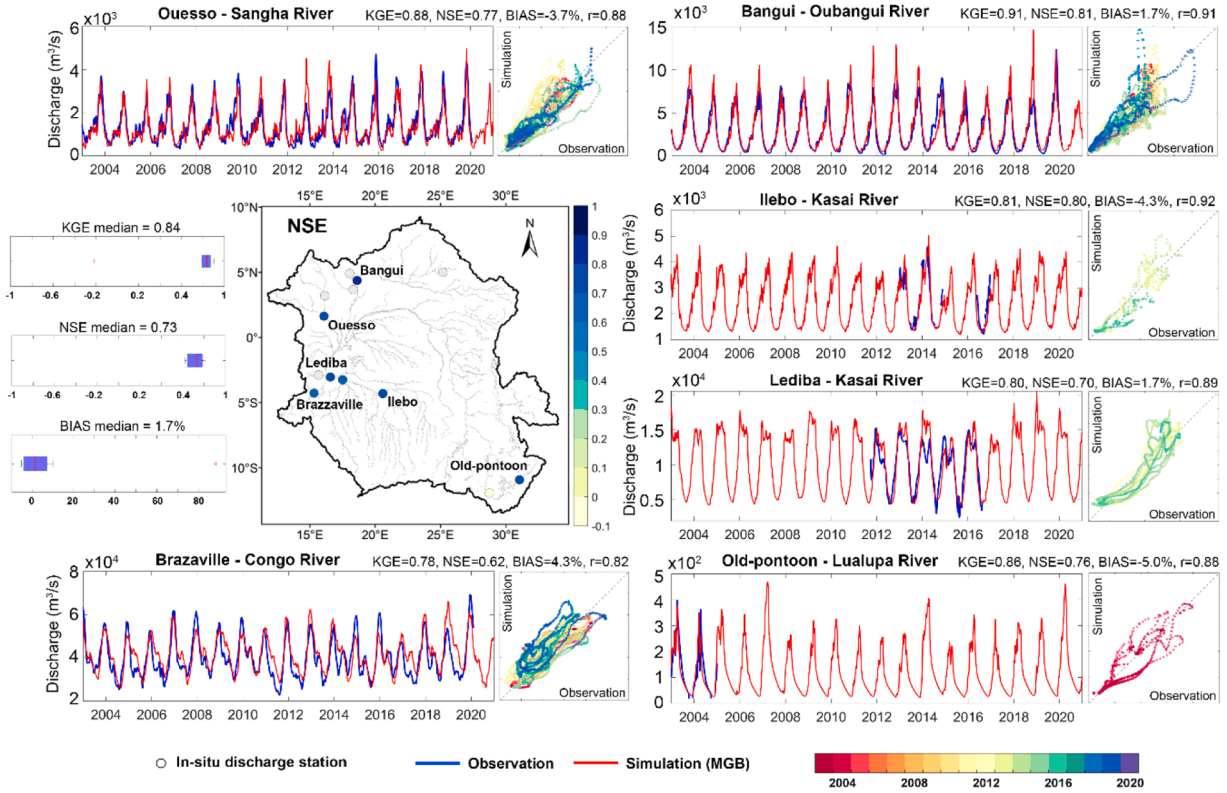

Fig. 4. Time series of observed (blue line) and simulated (red line) discharge for six in-situ stations for the calibration period 2001–2020. The scatterplot of the observed vs. simulated daily series with the colors of each point corresponding to the respective year is placed next to the time series. The spatial distribution and the boxplot of the statistical performance index for in-situ gauges are shown in the middle-left panel.

calibration period. The overall performance for NSE and Pearson correlation coefficient r are 0.38 and 0.75, respectively. A better performance is shown for the northern and southern (i.e. Kasai River) tributaries of the CRB. The time series of water level anomaly show a satisfactory agreement between MGB simulations and remote sensing-based observations, considering amplitude, interannual and seasonal representation for most of the basin. The lowest performance is found in the Middle-Congo region (e.g. Lopori and Ruki rivers), which may be likely due to two causes: i) the low representativeness of the annual variability of rainfall in the central Congo region as assessed by (Beck et al., 2017) when analyzing several rainfall datasets including CHIRPS used in this study; ii) although the hydraulic parameters of the main channel were calibrated (depth and width), the floodplain topography (MERIT DEM) used to generate the hypsometric curve is probably not sufficiently accurate in representing the bare surface since this region is particularly covered by dense forest, as seen in the land use-land cover maps (see Fig. S3b-c in the Supplementary material).

Regarding the time series and spatial distribution of the discharge during the validation period (1981–2000), KGE, NSE and relative bias show a median value of 0.71, 0.51 and −11.7%, respectively (Fig. 6). Similar to the calibration period, the better performance is captured for the northern region of the CRB (Sangha and Oubangui), where interannual and seasonal variability are adequately represented. Overall, the model performance for the timing and magnitude of high and low flows is better that those obtained in previous studies (i.e. (Dos Santos et al., 2022; Paris et al., 2022, p. 202; Tshimanga and Hughes, 2014). The validation of in-situ water level anomaly is shown in Fig. S6. For comparison purposes with other hydrological-related variables, the terrestrial water storage from GRACE (Rodell and Famiglietti, 2002; Scanlon et al., 2016; Strassberg et al., 2009) and surface water extent from GIEMS-2 (Papa et al., 2010; Prigent et al., 2007) are also assessed and are shown in the supplementary material (Figs. S7 and S8).

3.1.2. *Representation of lake dynamics*

Fig. 7a shows the monthly mean climatology of discharge for historical records from in-situ stations downstream of four lakes compared to the MGB simulation results. Lake Tanganyika shows the best performance considering the relative bias and Pearson correlation coefficient of − 1.3% and 0.97, respectively. In addition, while the simulation of the seasonality is satisfactory for the lakes Mweru and Zimzambo there is an overestimation of the discharges by the model. For Lake Kivu, there is a significant flow underestimation, mainly during the dry season, likely because it is a regulated lake and, therefore, there is a controlled flow during the dry

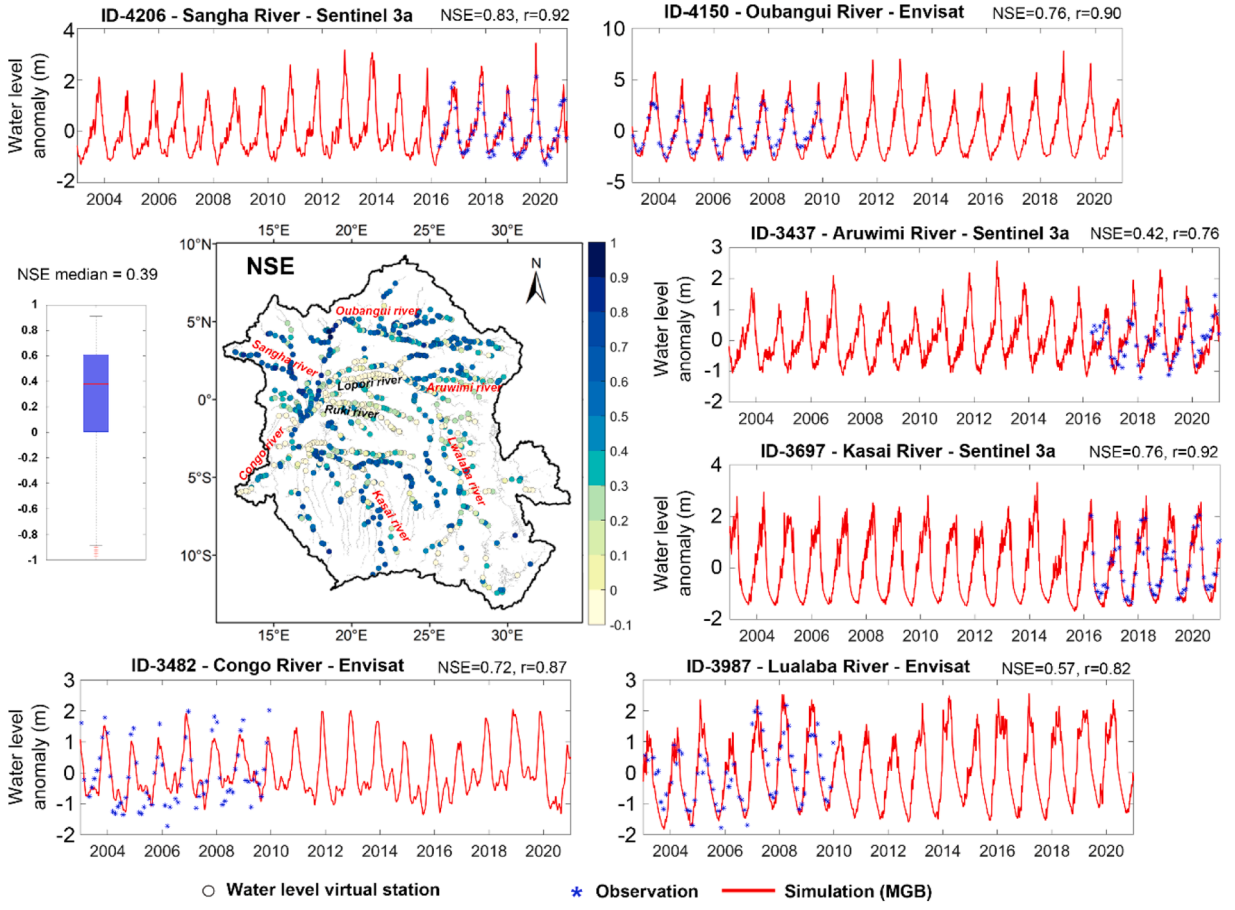

Fig. 5. Time series of observed (blue dots) and simulated (red line) water level for 836 virtual stations for the calibration period 2001–2020. The spatial distribution and the boxplot of the Nash–Sutcliffe efficiency index for virtual stations is shown in the middle-left panel.

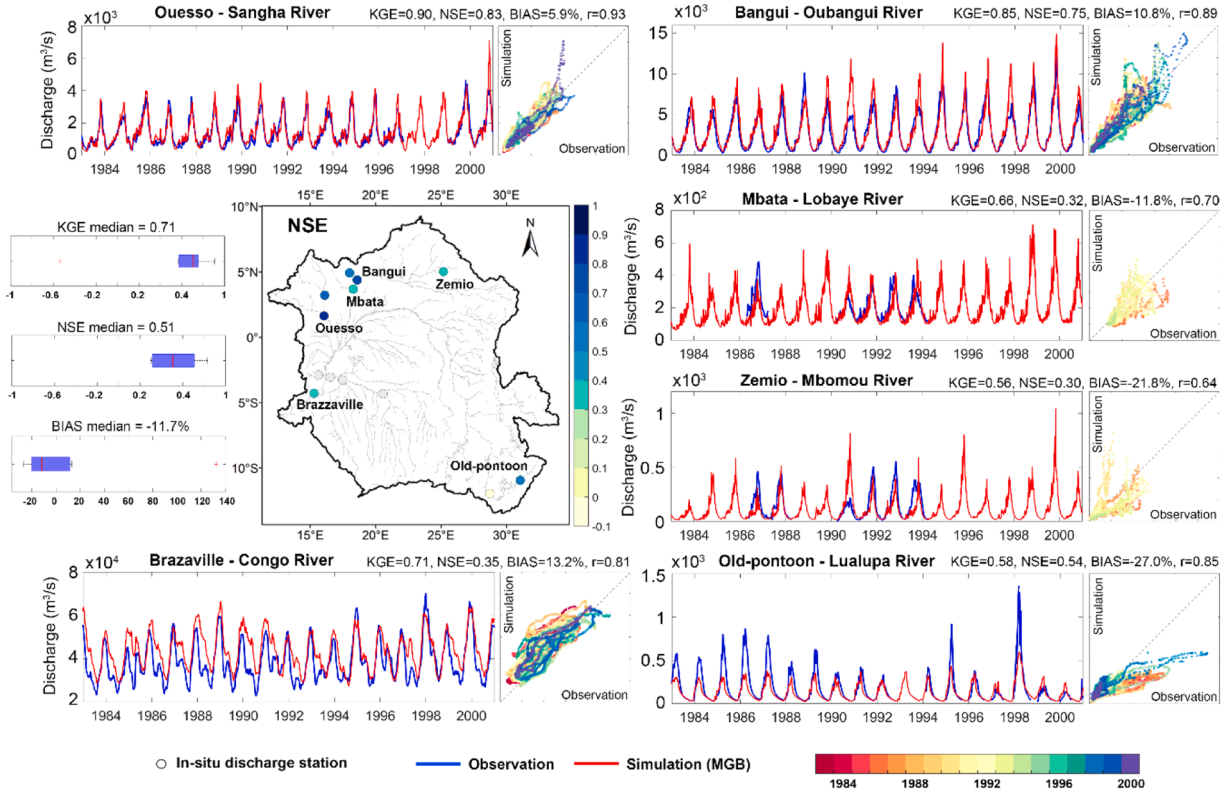

Fig. 6. Time series of observed (blue line) and simulated (red line) discharge for six in-situ stations for the validation period 1981–2000. The scatterplot of the observed vs. simulated daily series with the colors of each point corresponding to the respective year is placed next to the time series. The spatial distribution and the boxplot of the statistical performance index for in-situ gauges are shown in the middle-left panel.

season. In general, it has been possible to capture the climatology of discharges in four lakes, especially when compared to the model run without representation of lakes. It must be noticed also that biases can arise because the simulation and observations come from two different periods that are 50 years apart. In general, the implementation of lakes in MGB during the calibration period had an impact on the discharge series which can be seen for the ratio between the discharge with and without lakes for each river reach (upper center Fig. 7a). It has been observed that more than 95% of the river reaches vary in discharge by $\pm$ 10% when the lake module is incorporated (see the histogram in the lower center Fig. 7a). The greatest influence is observed in the Lualaba region where there is a greater number of lakes that influence this process simulated in the MGB. This reduction is most evident downstream of Lake Tanganyika where the volume reduction can almost double. The circles in Fig. 7 show the calibration stations where there is a significant reduction in RRMSE for three out of the five historical stations (downstream of Tanganyika, Mweru and Zimzambo lakes). For the validation period, Fig. 7b shows the time series of the water level anomaly represented by the MGB model simulation with and without representation of lakes, and water level anomalies from radar altimetry. In general, there is an improvement in the amplitude and timing of the anomalies. Pearson correlation coefficient is improved, moving from 0.3 to 0.68, and NSE improved from -0.7 to 0.33 when the lake scheme is used (Fig. 7c). In previous studies (e.g. (Paris et al., 2022), lakes Mweru and Tanganyika, for example, were not properly modeled, and in fact their discharge outflows were directly forced/substituted by virtual discharge time series, which is defined as a series constructed from satellite altimetry and in-situ historical information.

3.1.3. Long-term simulation and validation of the assimilation scheme

A 40-year time series of hydrological variables is generated with MGB, for the period 1981–2020 (Fig. 8), using both the new representation of the lake storage dynamics and the LEnKF data assimilation scheme (experiment S.1; see Fig. 3). The performance metrics (NSE, KGE and Pearson correlation coefficient) for discharge time series are 0.61, 0.73 and 0.87, respectively, which are satisfactory for a 40-year long simulation at daily time scale. There is also an improvement in the RRMSE of 13% (reduction of errors) for validation the discharge temporal series. Overall, the bimodal behavior of the discharge series at Lediba and Brazzaville stations is well captured by MGB. However, there are still maximum annual events where MGB simulations overestimate the observations, e.g. for the north-western part at Salo and Ouesso stations in 2000, and the northern region at Bangui and Zemio stations in 2003. This behavior is specific only during these years, which could be explained by the poor representativeness of CHIRPS precipitation of these events. Similar performance is shown when the in-situ water levels are used for validation (see Fig. S6 in the Supplementary material).

Results of experiment S.2 (see Fig. 3) are shown in Fig. 9, for which the three longest series of discharges and water levels are used

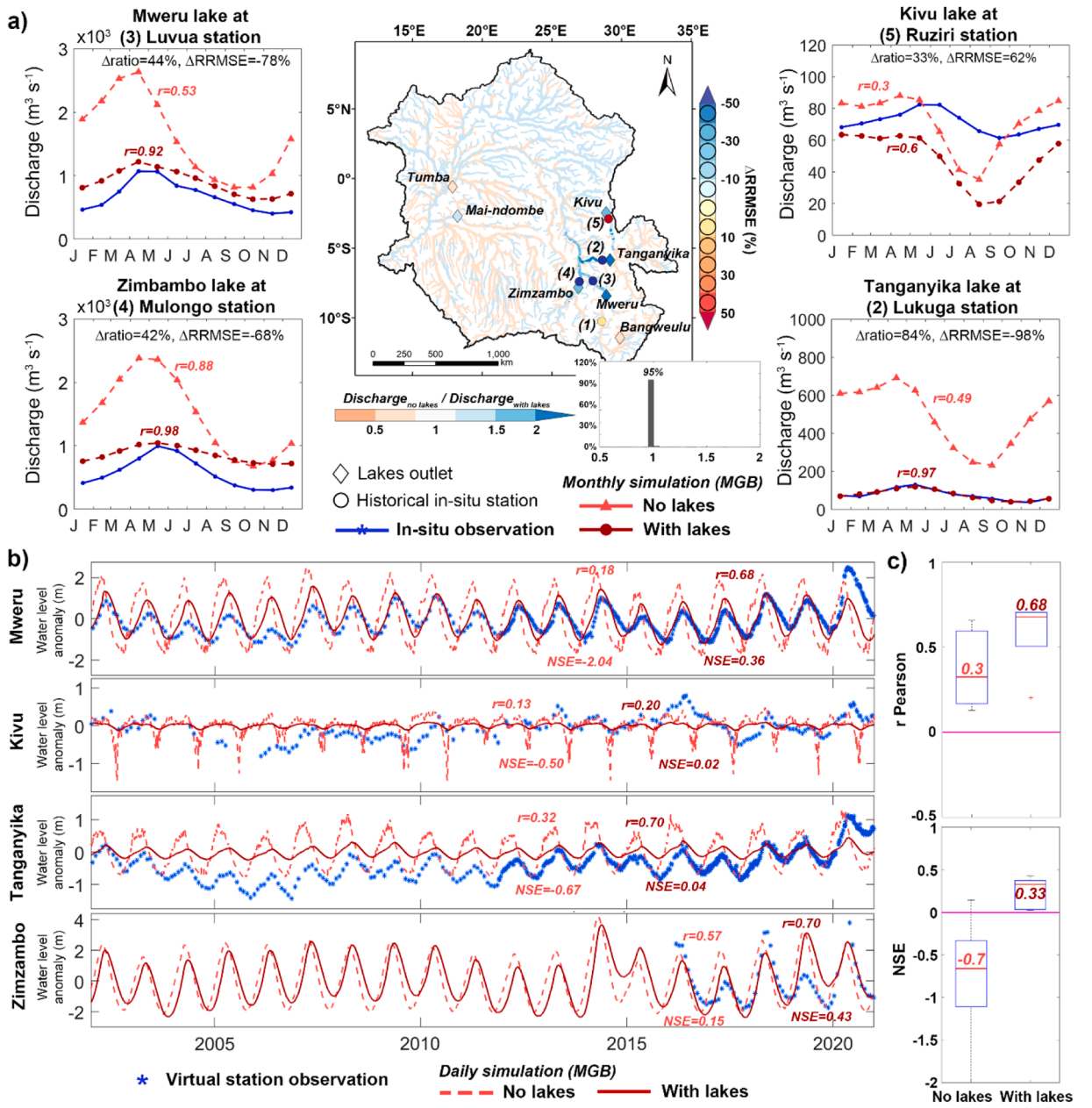

Fig. 7. (a) Time series of the observed (blue, 1950–1959) and simulated discharge climatology without lakes (light red) and with lakes (dark red) implementation for 2001–2020 at four stations downstream of the lakes used for calibration (circles) represented on the map with the ΔRRMSE index from red to blue palette color. The central map shows the ratio of mean discharge without lakes to discharge with lakes for each river reach and each lake (diamonds). The histogram of this ratio for all river reaches is shown next to the map. (b) Time series of satellite derived water level anomaly (blue dots) and simulated water level anomaly from MGB without (light red) and with lakes (dark red) implementation during the phase of validation (2001–2020) at same lakes used during calibration phase. (c) Boxplot of Pearson correlation coefficient r and NSE index during validation period for simulated water level anomaly from MGB without (light red) and with lakes (dark red) implementation.

for validation. In general, there is an improvement in the RRMSE of almost 14% for validation of discharge time series. The largest improvement is observed in the Oubangui region at the Bangui station with a reduction in RRMSE of ~17%. Improvements are also found downstream at the Brazzaville station. For the assimilated stations improvements are even greater, reaching a RRMSE reductions of ~70% at some stations (e.g., Salo, Zemio, Mbata and Dimalumbu). Validation with in-situ water levels for experiments S.1 and S.2 is shown in Figs. S9 and S10, respectively. The LEnKF implementation improves the water level simulations when compared to the 836 VSs, from mean NSE values of 0.38–0.5 (see Fig. S11). The cross-validation in Experiments S.1 and S.2 shows that the LEnKF method performs satisfactorily in improving the discharge time series from MGB in different regions of the CRB. With this satisfactory

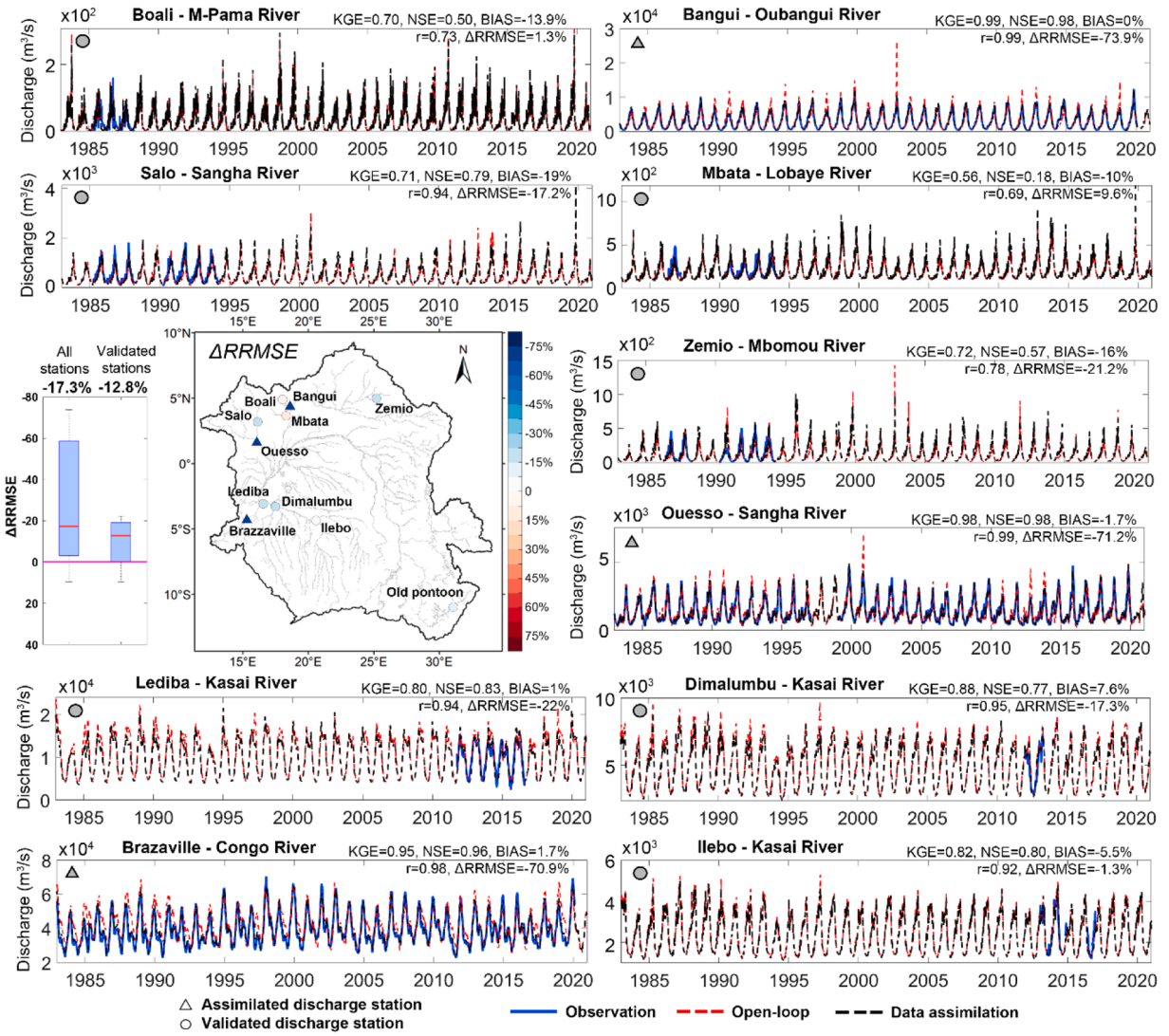

Fig. 8. Time series of observed (blue line), open-loop simulation (dashed red line) and assimilated simulation (dashed black line) discharge for three assimilated (triangles) and seven validated (circles) in-situ stations for the long-term period 1981–2020. The spatial distribution and the boxplot of the ΔRRMSE performance index for in-situ gauges are shown in the middle-left panel.

performance, experiment S.3 is implemented by assimilating all the existing information which will allow us to analyze the extreme hydrological events in the CRB at a spatially and temporally distributed level.

3.1.4. Hydrological extreme events analysis and ENSO teleconnections

This section analyzes specific extreme hydrological events identified through MGB simulations and observations in the CRB. For this purpose, we use the experiment S.3 (see Fig. 3), in which all available in-situ observations of discharge and water level as well as radar altimetry have been assimilated; and this scenario correspond to the so-called CRB hydrological reanalysis. The performance achieved with this experiment (S.3) was analyzed with respect to the observed discharge at all stations showing a median NSE, KGE and Pearson correlation coefficient of 0.95, 0.94 and 0.98 respectively. Considering the in-situ water level anomaly, the NSE and Pearson correlation coefficient are 0.65 and 0.92, respectively. It should be noted that this high performance is also due to the fact that the simulations are being evaluated with the same in-situ series used for assimilation. If we analyze the water level from VSs, the NSE and Pearson correlation coefficient values are 0.50 and 0.82, respectively. This last value can be compared with previous studies (e.g. (Paris et al., 2022) that reached a Pearson correlation coefficient of 0.74 for the median of the VSs evaluated.

This long-term reanalysis allows us to evaluate potential climate drivers of extreme hydrological events in the CRB, in particular with respect to ENSO, the strongest mode of large-scale interannual climate variability. It is well-known that ENSO-related shifts in SST in the Pacific lead to changes in the Walker circulation, which in turn leads to a significant redistribution of deep atmospheric convection in the tropics. As a result, ENSO can exert a strong influence on large-scale precipitation patterns, and particularly on the

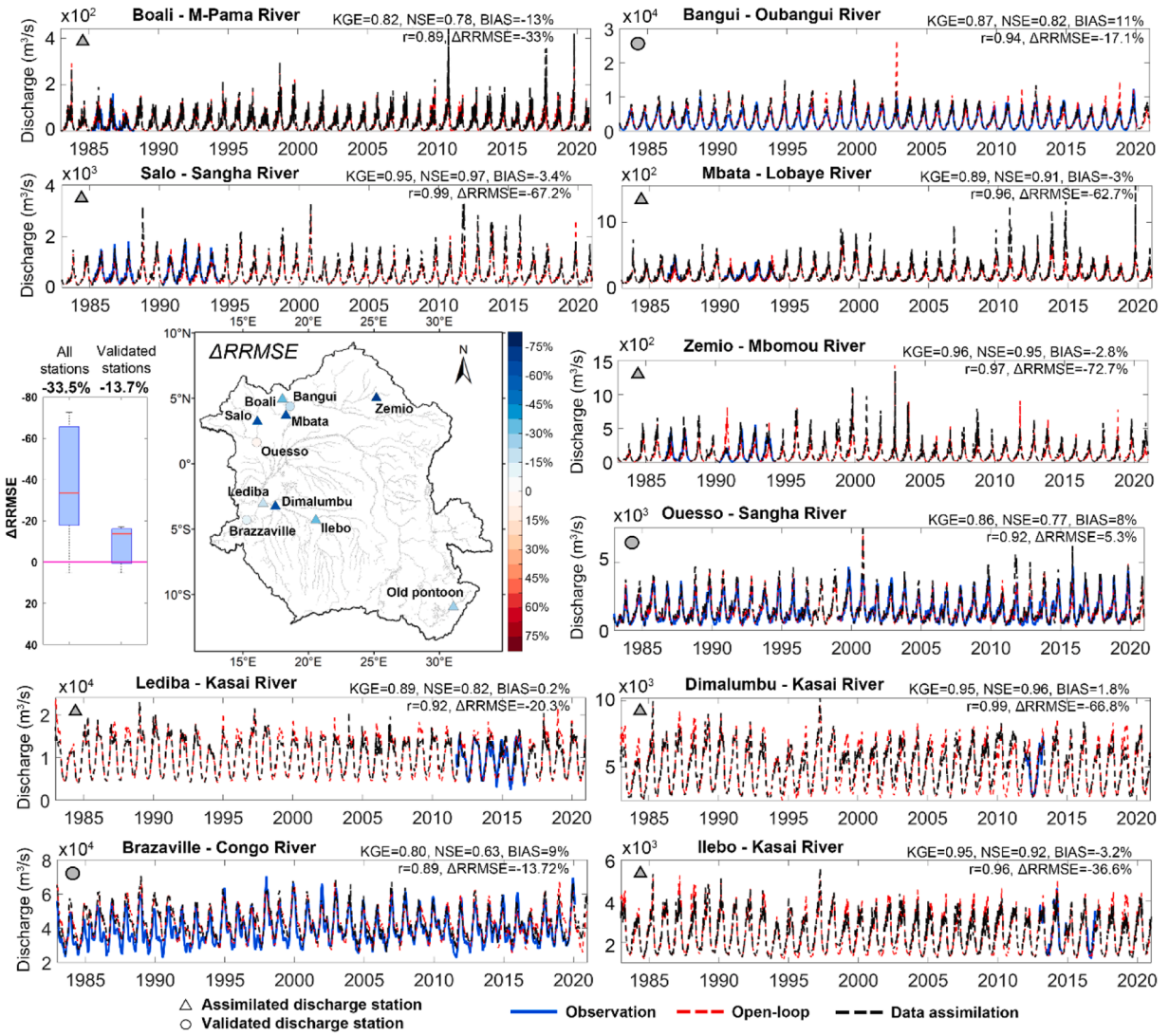

Fig. 9. Time series of observed (blue line), open-loop simulation (dotted red line) and assimilated simulation (dotted black line) discharge for seven assimilated (triangles) and three validated (circles) in-situ stations for the long-term period 1981–2020. The spatial distribution and the boxplot of the ΔRRMSE performance index for in-situ gauges are shown in the middle-left panel.

strength of monsoonal systems (Taschetto et al., 2020). For instance, at the peak of El Niño, the East Asian, North American, and West African monsoons are significantly strengthened, while the South American monsoon is weakened. These changes in precipitation patterns typically correspond to changes in the amount of freshwater flowing from rivers to the ocean. Here we evaluate ENSO by using the Niño-3.4 SST index (i.e., SST anomalies averaged in the region delineated by the magenta rectangle on Fig. 10a).

The duration and intensity of extreme events are shown in Fig. 10b-c for the flood years of 1997–1998 and 2019–2020, and for the drought years of 1983–1984 and 2011–2012, respectively. These events were selected by considering the station with the largest drainage area (Brazzaville) and the events that affected the largest areas across CRB (see Figs. S12 and S13). Fig. 10d shows the interannual discharge anomalies from observations (blue) and hydrologic reanalysis (dotted black) at four in-situ stations. A mean Pearson correlation coefficient of 0.96 and 0.77 is found for the three stations with the longest series and for all 13 in-situ discharge stations, respectively. This can be considered a satisfactory performance considering 40-years of daily discharge simulation. Fig. 10b-c show that the flood events occurred mainly in the main stem and in the Lualaba (Kasai's headwater for 2019–2020) region in the south-eastern (southern) part of the CRB, considering duration and intensity exceeding 90 days and 50 years of return period, respectively. Specifically for the 1997–1998 year, a strong El Niño event was recorded (vertical opaque red bar in Fig. 10d) with a duration of approximately 13 months. This occurred in the same time that large floods were detected at the Bangui and Brazzaville stations by observations and MGB simulations. The 1997–1998 Super El Niño event also caused extreme hydrological events in the Amazon, but these were extreme droughts rather than floods as in the CRB (Marengo et al., 1998; Marengo and Espinoza, 2016), highlighting a different hydrological response in the Atlantic and therefore distinct ENSO teleconnection pathway leading to flooding in the CRB. The

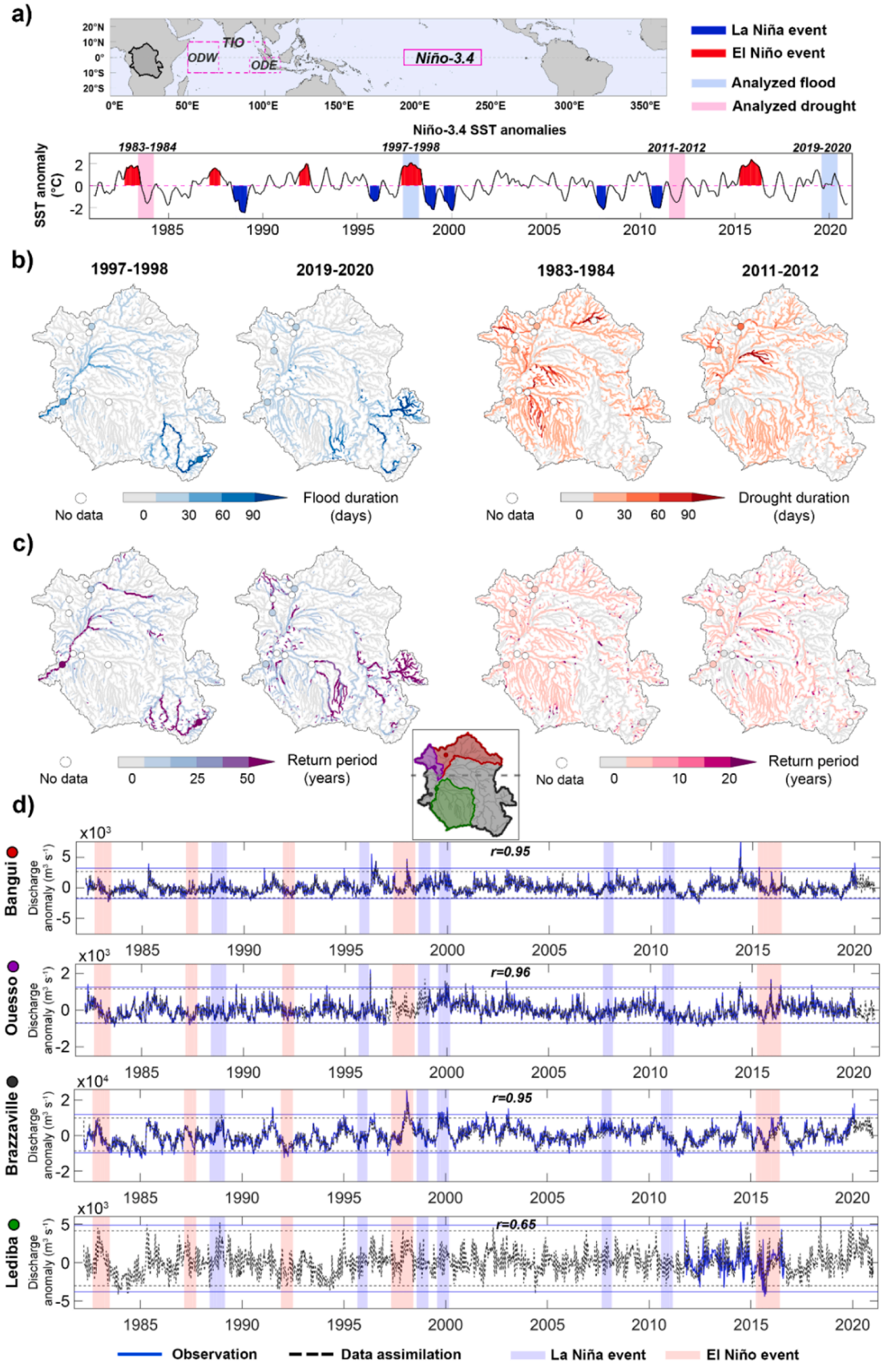

(caption on next page)

Fig. 10. (a) Map of the global tropical zone with the Niño-3.4 region (magenta rectangle), the TIO and western (ODW) and southeastern (ODE) TIO regions (dotted magenta rectangle) and the Congo River basin (black polygon). Time series of Niño-3.4 SST anomalies. Blue and red filled areas indicate La Niña and El Niño events respectively. (b) Maps of the number of days during flood and drought periods in blue and red palettes, respectively, for specific events. The results of the MGB simulations are shown in each river reach and the observations are shown in circles. (c) Maps of intensity of flood and drought events in blue-purple and red-purple palettes, respectively, expressed in return period in years and for the same events selected in (b). (d) Time series of interannual discharge anomalies from observations (blue) and MGB simulation (dashed black) for the three stations with the most extensive data. Horizontal lines represent estimated thresholds for observations and simulations. The opaque vertical bars represent La Niña (blue) and El Niño (red) events. The map of the regions (colored borders and circles) to which these series belong is shown in the upper center of this panel.

2019 event was also documented in the Ubangui region (Gosset et al., 2023). However, there is no evidence that the 2019–2020 year is related to an extreme El Niño event, although the Niño-3.4 SST index experienced positive values during the boreal winter before turning negative again, leading the climate condition in the Pacific towards a rare triple-dip La Niña. One can note that the classic "double-dip" usually follows extreme El Niño events such as the one of 2015–2016 (e.g., Hu et al., 2014; Iwakiri and Watanabe, 2021; Wu et al., 2019).

In terms of drought, the 1983–1984 event is observed at the three stations with the longest records, of which Bangui and Ouesso are influenced by the northern regions of the CRB. This extreme event has been documented by Adisa et al. (2019) and Masih et al. (2014); the latter analyzed the droughts between 1900 and 2013, and detected the 1983–1984 drought as a continental scale event and unique in the period analyzed. This event is spatially represented by the MGB simulations in each river reach. This drought has also been simulated in the Kasai region in the southern part of the CRB with duration values exceeding 90 days. This event occurs at the end of a La Niña event in 1983–84 that followed the extreme 1982–1983 El Niño event (Fig. 10d). The 2011–2012 drought event was also recorded by observations at the same stations in Bangui, Ouesso and Brazzaville, as well as by MGB and occurred a few months after a major La Niña event that peaked during the 2011/12 boreal winter (Fig. 10d).

To further evaluate the potential teleconnection between ENSO variability and precipitation/flooding patterns in the CRB region, we present, in Fig. 11, composite maps of standardized discharge anomalies, during strong La Niña (Fig. 11a) and El Niño (Fig. 11b) events, i.e. periods when the Niño-3.4 SST index is below and above one standard deviation, respectively. In the northern region, events of maximum values of the normalized discharge anomaly are mainly associated with La Niña periods (see composite in Fig. 11a) while the minimum values occur mainly during periods of strong El Niño (Fig. 11b). Interestingly, opposite patterns can be found in the Southern region. Because ENSO exhibits a clear seasonal phase locking (Stein et al., 2014), characterized by a strong tendency for events to peak in the boreal winter, ENSO's impacts have been shown to be seasonally modulated (e.g., Almar et al., 2022; Boucharel et al., 2021). This could explain the opposite precipitation response to ENSO events of the southern and northern Congo, which is located across the equator and therefore exhibits an out-of-phase climatology between its northern and southern regions (see Fig. 7a).

In addition, Fig. 11c shows the Pearson correlation coefficient (with a significance level of 0.05) between the monthly series of discharge anomalies and the Niño-3.4 SST index. The highest values are located in the upper part of the Middle Congo and Kasai regions where the time lag where this maximum correlation occurs varies from zero to approximately 4 months (Fig. 11d). Additionally, another region that shows relatively high correlations in this analysis is the northern region with a lag of 11–12 months (Fig. 11d). This is especially true for the two extreme drought events of 1983–1984 and 2011–2012. As the patterns of teleconnections and their associated impacts differ significantly between the onset and decay phases of ENSO events (Sprintall et al., 2020; Taschetto et al., 2020), this could explain why these droughts can occur with a lag of up to one year, probably due to a cumulative effect, as already reported by (Lv et al., 2022) when they analyzed the relationship between ENSO events and droughts in China.

Although the present analysis clearly highlights a strong teleconnection between ENSO variability and regional patterns of river discharge in the CRB, it also shows that the teleconnection is far from linear and straightforward, with a potentially strongly seasonally modulated and delayed precipitation response to ENSO events of different amplitude as shown in Fig. S14 in the Supplementary material, where seasonal correlations are negative mainly in the northern regions of the CRB (Sangha and Ubangui regions). In addition, the Dry Years (DJF) in the northern CRB region are highly correlated with SST variability in the Indo-Pacific, that has been corroborated by analyzing the seasonal correlations between the TIO SST anomaly and the discharge series (see Fig. S16 in the Supplementary material). Additionally, there is a high correlation during the beginning of the dry period (MAM) in the southeastern CRB region (Lualaba region). (Moihamette et al., 2022) found that about 20–32% of the rainfall variance in the CRB is associated with the Indian Ocean dipole (IOD), independent of El Niño or La Niña, between the November and December periods. This has been verified in this study by analyzing the DMI index where the highest correlations with the discharge series are found in the Middle Congo and Lualaba regions with a time lag of zero months, i.e. an almost immediate impact (see Fig. S17 in the Supplementary material). At the seasonal level, there is a high significant correlation during the dry period (DJF) in the Ubangui region and during the onset of wet period (SON) in the Lualaba region. Despite these high correlations, the DMI index is only able to explain the 1997–1998 flood, similar to the way the ENSO index does in this particular event. However, these analyses suggest that ENSO explains a greater teleconnection with the major flood and drought events in the last 40 years in the CRB than TIO SST and DMI index.

This is an illustration of the complex inter-basin climate teleconnections to discharge patterns in tropical Africa, which definitely requires more thorough investigation, especially to disentangle the impacts from the different modes of interannual tropical variability (e.g., ENSO, IOD) and/or low-frequency climate indices (e.g. Atlantic Multidecadal Oscillation (AMO), Solar activity changes, among others) as studied by Lüdecke et al. (2021).

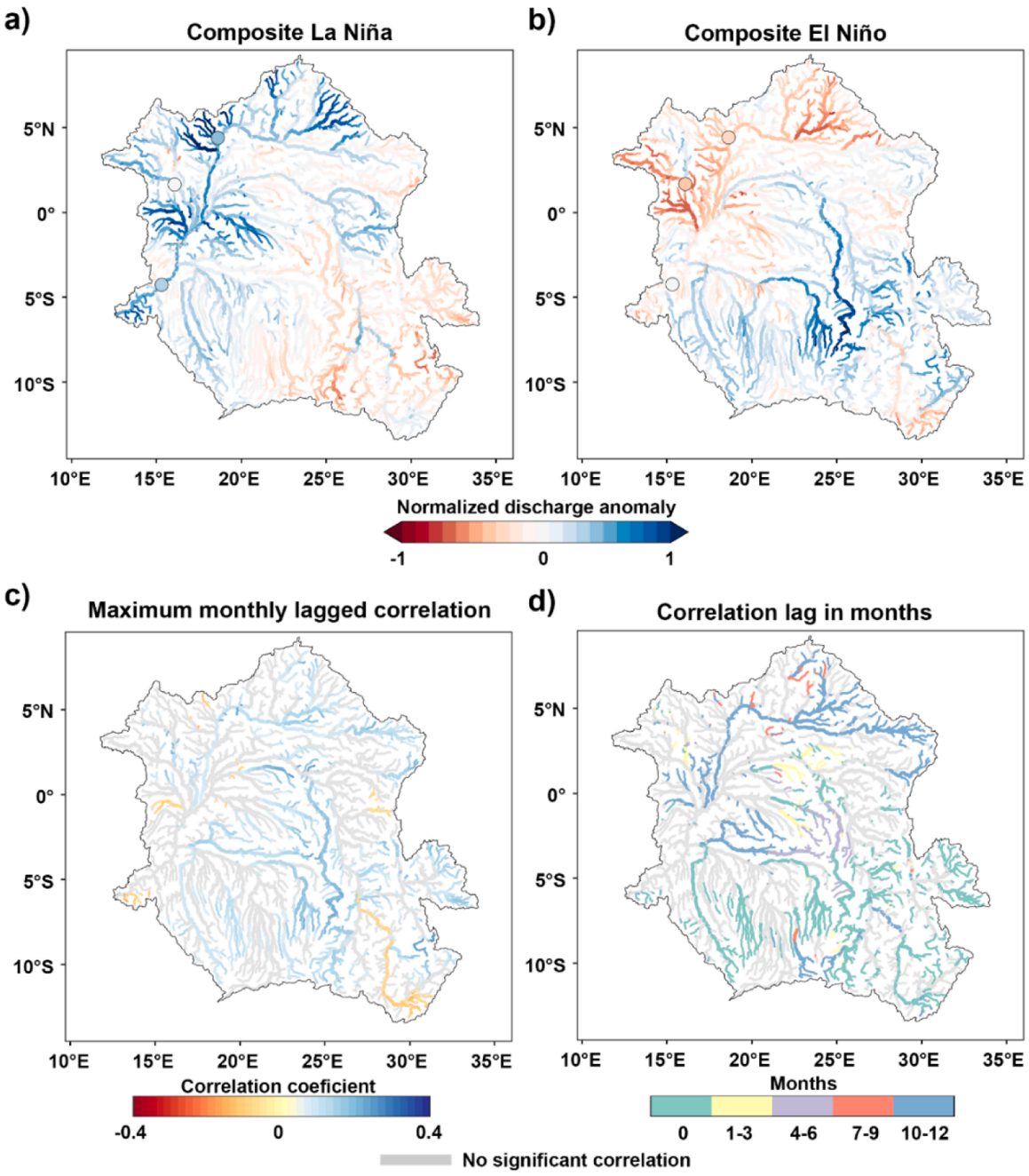

Fig. 11. Map of composites of the normalized discharge anomaly during (a) La Niña and (b) El Niño events in the 1981–2020 period. (c) Maximum monthly lagged Pearson correlation coefficient between the Niño-3.4 SST anomaly series and the discharge anomaly, with a significance level of 0.05, and (d) the monthly lag at which this maximum correlation occurs.

4. Conclusions

This study presents an improved and coherent long-time series of simulated daily discharges for the whole Congo River basin (CRB) for the period 1981–2020. Simulation improvements were supported by the representation of the dynamics of seven major lakes, which is an important yet overlooked process in large-scale models of the CRB where only the outflows in each lake were replaced. Complementarily, a data assimilation technique was able to further improve discharge simulations across the basin. The dynamics of the discharges over the CRB was analyzed with a main focus on the spatial and temporal distribution of extreme hydrological events and its relationship with large-scale climatic factors, specifically with ocean temperature from the El Niño-Southern Oscillation

(ENSO).

The performance of the discharge simulations was evaluated on a daily basis. Three steps were considered: 1) the calibration of the MGB model hydrologic and hydraulic parameters, yielding an average performance of 0.71 considering the KGE index; 2) the calibrated lake scheme, which showed an average improvement in performance from 0.3 (without the scheme) to 0.68 (with the scheme), for Pearson's correlation coefficient; 3) correction of long-term time series with the LEnKF data assimilation framework. Two cross-validation experiments showed an improvement in RRMSE of about ~13% in the simulated discharges, and are satisfactory to represent the interannual and seasonal variability in the CRB, when compared to previous modeling studies, reaching NSE levels of e.g., 0.95 and 0.65 in the daily in-situ discharge and water level series, respectively, for the last experiment called hydrological reanalysis.

Several historical flood and drought events were also evaluated based on the long-term run with representation of lake storage dynamics and data assimilation named hydrological reanalysis from the CRB. A high correlation between the observed and simulated series allowed us to have a satisfactory degree of confidence to identify extreme events also in places where there are no observations. Two major droughts and floods were evaluated. The flood of 1997–1998 was mainly associated with a major El Niño in the same period, however for the event of 2019–2020 there was no evidence of its association with any temperature anomaly in the central Pacific (Niño-3.4 region). As for the 1983–1984 and 2011–2012 droughts that mainly affected the Ubangui and Sangha in the north and Kasai in the south region of the CRB, it is observed that they are highly correlated some months earlier by large El Niño and La Niña events, respectively. These events showed a significant correlation with a delay of 10–12 months for the northern region and the Niño-3.4 region.

These results show the spatial and temporal complexity of the teleconnections between hydrology and large-scale climate phenomena such as the ENSO and the Tropical Indian Ocean (TIO), giving us new insights such as the fact that river discharge in the CRB is not linearly related to the amplitude of the ENSO event, but which better explains higher extreme flood and drought events compared to TIO SST and DMI index during the last 40 years. This also gives us perspectives for SST analysis in other tropical ocean regions such as the Madden-Julian Oscillation. This is the first work that addresses these relationships in terms of discharge from a series of hydrological reanalysis for the second largest basin in the world.

In addition to having a long-term consolidated daily discharge base (or what could also be called the first hydrological reanalysis of the Congo in the last 40 years), the techniques implemented in the setup of the hydrological model could be used with an operational perspective, which is of great importance in the CRB, a region that has limited in-situ information and is under threats to ongoing climatic changes and anthropogenic pressure.

CRediT authorship contribution statement

Kitambo Benjamin: Writing – review & editing, Investigation. **Papa Fabrice:** Writing – review & editing, Supervision, Methodology, Investigation, Funding acquisition, Formal analysis, Conceptualization. **Paris Adrien:** Writing – review & editing, Supervision, Methodology, Funding acquisition, Formal analysis, Conceptualization. **Ayan Santos Fleischmann:** Writing - review & editing, Methodology, Investigation, Formal analysis. **Fleischmann Ayan:** Writing – review & editing, Investigation, Formal analysis. **Wongchuig Sly:** Writing – review & editing, Writing – original draft, Visualization, Validation, Methodology, Investigation, Formal analysis, Data curation, Conceptualization. **Tshimanga Raphael:** Writing – review & editing, Methodology, Investigation, Formal analysis. **Calmant Stéphane:** Writing – review & editing, Formal analysis. **Gal Laetitia:** Writing – review & editing, Methodology, Investigation, Data curation. **Boucharel Julien:** Writing – review & editing, Methodology, Investigation, Formal analysis. **Paiva Rodrigo:** Writing – review & editing, Methodology, Investigation, Formal analysis. **Oliveira Romulo Jucá:** Writing – review & editing, Formal analysis.

Declaration of Competing Interest

The authors declare that they have no known competing financial interests or personal relationships that could have appeared to influence the work reported in this paper.

Data availability

Data will be made available on request.
Hydrological Reanalysis for the Congo River Basin (1983–2020) (Original data) (Zenodo)

Acknowledgments

This research has been supported by the CNES TOSCA project "DYnamique hydrologique du BAssin du CoNGO (DYBANGO)" (2020–2023), the French Space Agency (CNES), the Agence Française du Développement (AFD) and the Institut de Recherche pour le Développement (IRD). The first author thanks João Paulo Lyra Fialho Brêda for discussions for the implementation of the lake routing module in the MGB model. The authors would also like to thank the following agencies/organizations for providing access to data: The Climate Hazards Group Infrared Precipitation for providing CHIRPS; the Jet Propulsion Laboratory (JPL), the University of Texas Center for Space Research (CSR) and the Geo Forschungs Zentrum (GFZ) Potsdam for providing GRACE; the Copernicus Climate

Change Service (C3S) for providing the ERA5 datasets; the National Oceanic and Atmospheric Administration (NOAA) for providing the time series of the Niño-3.4 SST index. The developed data, the improved 40-year (1981–2020) hydrological reanalysis of daily CRB discharge that support the findings of this study are available at Zenodo database: <10.5281/zenodo.8199770>.

Appendix A. Supporting information

Supplementary data associated with this article can be found in the online version at doi:10.1016/j.ejrh.2023.101563.

References

Adisa, O.M., Botai, J.O., Adeola, A.M., Botai, C.M., Hassen, A., Darkey, D., Tesfamariam, E., Adisa, A.T., Adisa, A.F., 2019. Analysis of drought conditions over major maize producing provinces of South Africa. J. Agric. Meteorol. 75, 173–182. https://doi.org/10.2480/agrmet.D-18-00049.

Almar, R., Graffin, M., Boucharel, J., Abessolo, G.O., Thoumyre, G., Papa, F., Montano, J., Bergsma, E., Baba, M.W., Jin, F.-F., Ranasinghe, R., 2022. El Niño controls the evolution of shorelines worldwide (preprint). in preparation. https://doi.org/10.21203/rs.3.rs-1283693/v1.

Alsdorf, D., Beighley, E., Laraque, A., Lee, H., Tshimanga, R., O'Loughlin, F., Mahé, G., Dinga, B., Moukandi, G., Spencer, R.G.M., 2016. Opportunities for hydrologic research in the Congo Basin. Rev. Geophys. 54, 378–409. https://doi.org/10.1002/2016RG000517.

An, S.-I., 2004. A dynamic link between the basin-scale and zonal modes in the Tropical Indian Ocean. Theor. Appl. Clim. 78, 203–215. https://doi.org/10.1007/s00704-003-0027-2.

Andreadis, K.M., Das, N., Stampoulis, D., Ines, A., Fisher, J.B., Granger, S., Kawata, J., Han, E., Behrangi, A., 2017. The regional hydrologic extremes assessment system: A software framework for hydrologic modeling and data assimilation. PLoS ONE 12, 1–22. https://doi.org/10.1371/journal.pone.0176506.

Anghel, C.G., Ilinca, C., 2023. Evaluation of various generalized pareto probability distributions for flood frequency Analysis. Water 15, 1557. https://doi.org/10.3390/w15081557.

Apers, S., Lannoy, G.D., Cobb, A.R., Dargie, G.C., Reichle, R.H., Bechtold, M., 2023. Insights into the hydrology of the Congo peatlands through land surface modeling and data assimilation (No. EGU23–6991). Presented at the EGU23, Copernicus Meetings. https://doi.org/10.5194/egusphere-egu23–6991.

Ayugi, B., Eresanya, E.O., Onyango, A.O., Ogou, F.K., Okoro, E.C., Okoye, C.O., Anoruo, C.M., Dike, V.N., Ashiru, O.R., Daramola, M.T., Mumo, R., Ongoma, V., 2022. Review of meteorological drought in Africa: historical trends, impacts, mitigation measures, and prospects. Pure Appl. Geophys. 179, 1365–1386. https://doi.org/10.1007/s00024-022-02988-z.

Balkema, A.A., de Haan, L., 1974. Residual life time at great age. Ann. Probab. 2, 792–804.

Bates, P.D., Horritt, M.S., Fewtrell, T.J., 2010. A simple inertial formulation of the shallow water equations for efficient two-dimensional flood inundation modelling. J. Hydrol. 387, 33–45. https://doi.org/10.1016/j.jhydrol.2010.03.027.

Beck, H.E., Vergopolan, N., Pan, M., Levizzani, V., van Dijk, A.I.J.M., Weedon, G.P., Brocca, L., Pappenberger, F., Huffman, G.J., Wood, E.F., 2017. Global-scale evaluation of 22 precipitation datasets using gauge observations and hydrological modeling. Hydrol. Earth Syst. Sci. 21, 6201–6217. https://doi.org/10.5194/hess-21-6201-2017.

Beighley, R.E., Ray, R.L., He, Y., Lee, H., Schaller, L., Andreadis, K.M., Durand, M., Alsdorf, D.E., Shum, C.K., 2011. Comparing satellite derived precipitation datasets using the Hillslope River Routing (HRR) model in the Congo River Basin. Hydrol. Process. 25, 3216–3229. https://doi.org/10.1002/hyp.8045.

Bhavani, T.S.D., Chowdary, J.S., Bharathi, G., Srinivas, G., Prasad, K.V.S.R., Deshpande, A., Parekh, A., Gnanaseelan, C., 2017. Response of the tropical Indian Ocean SST to decay phase of La Niña and associated processes. Dyn. Atmospheres Oceans 80, 110–123. https://doi.org/10.1016/j.dynatmoce.2017.10.005.

Biancamaria, S., Durand, M., Andreadis, K.M., Bates, P.D., Boone, A., Mognard, N.M., Rodríguez, E., Alsdorf, D.E., Lettenmaier, D.P., Clark, E.A., 2011. Assimilation of virtual wide swath altimetry to improve Arctic river modeling. Remote Sens. Environ. 115, 373–381. https://doi.org/10.1016/j.rse.2010.09.008.

Bola, G.B., Tshimanga, R.M., Neal, J., Trigg, M.A., Hawker, L., Lukanda, V.M., Bates, P., 2022. Understanding flood seasonality and flood regime shift in the Congo River Basin. Hydrol. Sci. J. 67, 1496–1515. https://doi.org/10.1080/02626667.2022.2083966.

Boucharel, J., Almar, R., Kestenare, E., Jin, F.-F., 2021. On the influence of ENSO complexity on Pan-Pacific coastal wave extremes. Proc. Natl. Acad. Sci. U.S.A. 118, e2115599118. https://doi.org/10.1073/pnas.2115599118.

Chambers, J.Q., Roberts, D.A., 2014. Drought in the Congo Basin. Nature 509, 36–37. https://doi.org/10.1038/nature13330.

Collischonn, W., Allasia, D., da Silva, B.C., Tucci, C.E.M., 2007. The MGB-IPH model for large-scale rainfall-runoff modelling. Hydrol. Sci. J. 52, 878–895. https://doi.org/10.1623/hysj.52.5.878.

Copernicus Climate Change Service, 2019. ERA5 monthly averaged data on pressure levels from 1979 to present. https://doi.org/10.24381/CDS.6860A573.

Datok, P., Fabre, C., Sauvage, S., N'kaya, G.D.M., Paris, A., Santos, V.D., Laraque, A., Sánchez-Pérez, J.-M., 2022. Investigating the Role of the Cuvette Centrale in the Hydrology of the Congo River Basin, in: Congo Basin Hydrology, Climate, and Biogeochemistry. American Geophysical Union (AGU), pp. 247–273. https://doi.org/10.1002/9781119657002.ch14.

Diem, J.E., Salerno, J.D., Palace, M.W., Bailey, K., Hartter, J., 2021. Teleconnections between rainfall in equatorial Africa and tropical sea-surface temperatures: a focus on Western Uganda. J. Appl. Meteorol. Climatol. https://doi.org/10.1175/JAMC-D-21-0057.1.

Dos Santos, V., Oliveira, R.A.J., Datok, P., Sauvage, S., Paris, A., Gosset, M., Sánchez-Pérez, J.M., 2022. Evaluating the performance of multiple satellite-based precipitation products in the Congo River Basin using the SWAT model. J. Hydrol.: Reg. Stud. 42, 101168 https://doi.org/10.1016/j.ejrh.2022.101168.

Emery, C.M., Paris, A., Biancamaria, S., Boone, A., Calmant, S., Garambois, P.A., Da Silva, J.S., 2018. Large-scale hydrological model river storage and discharge correction using a satellite altimetry-based discharge product. Hydrol. Earth Syst. Sci. 22, 2135–2162. https://doi.org/10.5194/hess-22-2135-2018.

Faragó, T., Katz, R.W., 1990. Extremes and design values in climatology. World Meteorological Organization (WMO), Geneva.

Fleischmann, A., Collischonn, W., Paiva, R., Tucci, C.E., 2019. Modeling the role of reservoirs versus floodplains on large-scale river hydrodynamics. Nat. Hazards 99, 1075–1104. https://doi.org/10.1007/s11069-019-03797-9.

Fleischmann, A.S., Paulo, J., Fialho, L., Wongchuig, S., 2021. Regional scale hydrodynamic modeling of the river-floodplain- reservoir continuum, 126114–126114 J. Hydrol.. https://doi.org/10.1016/j.jhydrol.2021.126114.

Folland, C.K., Palmer, T.N., Parker, D.E., 1986. Sahel rainfall and worldwide sea temperatures, 1901–85. Nature 320, 602–607. https://doi.org/10.1038/320602a0.

Funk, C., Peterson, P., Landsfeld, M., Pedreros, D., Verdin, J., Shukla, S., Husak, G., Rowland, J., Harrison, L., Hoell, A., Michaelsen, J., 2015. The climate hazards infrared precipitation with stations - A new environmental record for monitoring extremes. Sci. Data 2, 1–21. https://doi.org/10.1038/sdata.2015.66.

Gosset, M., Dibi-Anoh, P.A., Schumann, G., Hostache, R., Paris, A., Zahiri, E.-P., Kacou, M., Gal, L., 2023. Hydrometeorological extreme events in Africa: the role of satellite observations for monitoring pluvial and fluvial flood risk. Surv. Geophys. https://doi.org/10.1007/s10712-022-09749-6.

Hoerling, M., Hurrell, J., Eischeid, J., Phillips, A., 2006. Detection and attribution of twentieth-century northern and southern african rainfall change. J. Clim. 19, 3989–4008. https://doi.org/10.1175/JCLI3842.1.

Hosking, J.R.M., Wallis, J.R., 1987. Parameter and quantile estimation for the generalized Pareto distribution. Technometrics 29, 339–349. https://doi.org/10.2307/1269343.

Houtekamer, P.L., Mitchell, H.L., 2001. A sequential ensemble kalman filter for atmospheric data assimilation. Mon. Weather Rev. 129, 123–137. https://doi.org/10.1175/1520-0493(2001)129<0123:ASEKFF>2.0.CO;2.

Hu, S., Fedorov, A.V., Lengaigne, M., Guilyardi, E., 2014. The impact of westerly wind bursts on the diversity and predictability of El Niño events: An ocean energetics perspective. Geophys. Res. Lett. 41, 4654–4663. https://doi.org/10.1002/2014GL059573.
Huang, C., Zhang, Qiang, Xiao, Mingzhong, 2016. Influences of ENSO, NAO, IOD and PDO on precipitation regimes in the Pearl River basin. Acta Scientiarum Naturalium Universitatis Sunyatseni 2, 134–142. https://doi.org/10.13471/j.cnki.acta.snus.2016.02.023.
Iwakiri, T., Watanabe, M., 2021. Mechanisms linking multi-year La Niña with preceding strong El Niño. Sci. Rep. 11, 17465. https://doi.org/10.1038/s41598-021-96056-6.
James, R., Washington, R., Rowell, D.P., 2013. Implications of global warming for the climate of African rainforests. Philos. Trans. R. Soc. B: Biol. Sci. 368, 20120298. https://doi.org/10.1098/rstb.2012.0298.
Kabuya, P.M., Hughes, D.A., Tshimanga, R.M., Trigg, M.A., Bates, P., 2022. Assessing the potential value of the regionalised input constraint indices for constraining hydrological model simulations in the Congo River Basin. Adv. Water Resour. 159, 104093 https://doi.org/10.1016/j.advwatres.2021.104093.
Karam, S., Seidou, O., Nagabhatla, N., Perera, D., Tshimanga, R.M., 2022. Assessing the impacts of climate change on climatic extremes in the Congo River Basin. Clim. Change 170, 40. https://doi.org/10.1007/s10584-022-03326-x.
Katz, R.W., Parlange, M.B., Naveau, P., 2002. Statistics of extremes in hydrology. Adv. Water Resour. 25, 1287–1304. https://doi.org/10.1016/S0309-1708(02)00056-8.
Kelemen, Z., Gillikin, D.P., Borges, A.V., Tambwe, E., Sembaito, A.T., Mambo, T., Wabakhangazi, J.N., Yambélé, A., Stroobandt, Y., Bouillon, S., 2021. Freshwater bivalve shells as hydrologic archives in the Congo Basin. Geochim. Et. Cosmochim. Acta 308, 101–117. https://doi.org/10.1016/j.gca.2021.05.023.
Kitambo, B., Papa, F., Paris, A., Tshimanga, R.M., Calmant, S., Fleischmann, A.S., Frappart, F., Becker, M., Tourian, M.J., Prigent, C., Andriambeloson, J., 2022. A combined use of in situ and satellite-derived observations to characterize surface hydrology and its variability in the Congo River basin. Hydrol. Earth Syst. Sci. 26, 1857–1882. https://doi.org/10.5194/hess-26-1857-2022.
Kouakou, C., Paturel, J.-E., Satgé, F., Tramblay, Y., Defrance, D., Rouché, N., 2023. Comparison of gridded precipitation estimates for regional hydrological modeling in West and Central Africa. J. Hydrol.: Reg. Stud. 47, 101409 https://doi.org/10.1016/j.ejrh.2023.101409.
Laraque, A., N'kaya, G.D.M., Orange, D., Tshimanga, R., Tshitenge, J.M., Mahe, G., Nguimalet, C.R., Trigg, M.A., Yepez, S., Gulemvuga, G., 2020. Recent Budget of Hydroclimatology and Hydrosedimentology of the Congo River in Central Africa. Water 12, 2613. https://doi.org/10.3390/w12092613.
Liu, Y., Weerts, A.H., Clark, M., Hendricks Franssen, H.J., Kumar, S., Moradkhani, H., Seo, D.J., Schwanenberg, D., Smith, P., Van Dijk, A.I.J.M., Van Velzen, N., He, M., Lee, H., Noh, S.J., Rakovec, O., Restrepo, P., 2012. Advancing data assimilation in operational hydrologic forecasting: Progresses, challenges, and emerging opportunities. Hydrol. Earth Syst. Sci. 16, 3863–3887. https://doi.org/10.5194/hess-16-3863-2012.
Liu, Y., Wang, W., Hu, Y., Cui, W., 2016. Improving the distributed hydrological model performance in upper huai river basin: using streamflow observations to update the Basin States via the Ensemble Kalman Filter. Adv. Meteorol. 2016. https://doi.org/10.1155/2016/4921616.
Lüdecke, H.-J., Müller-Plath, G., Wallace, M.G., Lüning, S., 2021. Decadal and multidecadal natural variability of African rainfall. J. Hydrol.: Reg. Stud. 34, 100795 https://doi.org/10.1016/j.ejrh.2021.100795.
Lv, A., Fan, L., Zhang, W., 2022. Impact of ENSO events on droughts in China. Atmosphere 13, 1764. https://doi.org/10.3390/atmos13111764.
Mabrouk, E.H., Moursy, F.I., Morsy, M.M.A., 2022. Assessment of climate characteristics and long-term trends of rainfall and drought in the Congo River Basin. J. Water Clim. Change jwc2022241. https://doi.org/10.2166/wcc.2022.241.
Marengo, J.A., Espinoza, J.C., 2016. Extreme seasonal droughts and floods in Amazonia: causes, trends and impacts: EXTREMES IN AMAZONIA. Int. J. Clim. 36, 1033–1050. https://doi.org/10.1002/joc.4420.
Marengo, J.A., Nobre, C.A., Sampaio, G., 1998. On the associations between Hydrometeorological conditions in Amazonia and the extremes of the Southern Oscillation. Bull. De. l'Institut Fr. d'Études Andin. 27, 789–802. https://doi.org/10.3406/bifea.1998.1332.
Marengo, J.A., Borma, L.S., Rodriguez, D.A., Pinho, P., Soares, W.R., Alves, L.M., 2013. Recent extremes of drought and flooding in Amazonia: vulnerabilities and human adaptation. Am. J. Clim. Change 02, 87–96. https://doi.org/10.4236/ajcc.2013.22009.
Masih, I., Maskey, S., Mussá, F.E.F., Trambauer, P., 2014. A review of droughts on the African continent: a geospatial and long-term perspective. Hydrol. Earth Syst. Sci. 18, 3635–3649. https://doi.org/10.5194/hess-18-3635-2014.
Moihamette, F., Pokam, W.M., Diallo, I., Washington, R., 2022. Extreme Indian Ocean dipole and rainfall variability over Central Africa. Int. J. Climatol. 42, 5255–5272. https://doi.org/10.1002/joc.7531.
Moradkhani, H., 2008. Hydrologic remote sensing and land surface data assimilation. Sensors 8, 2986–3004. https://doi.org/10.3390/s8052986.
Mugisho Bachinyaga, J., Deijns, A., Ilombe Mawe, G., Kervyn, F., Michellier, C., Mugaruka Bibentyo, T., Nkere Buliba, J., Nzolang, C., Smets, B., Dewitte, O., 2022. The flash floods of April 2020 in Uvira (DR Congo): story of an event with extreme impacts (other). display. https://doi.org/10.5194/egusphere-egu22-6223.
Munzimi, Y.A., Hansen, M.C., Asante, K.O., 2019. Estimating daily streamflow in the Congo Basin using satellite-derived data and a semi-distributed hydrological model. Hydrol. Sci. J. 64, 1472–1487. https://doi.org/10.1080/02626667.2019.1647342.
Nadarajah, S., Shiau, J.T., 2005. Analysis of extreme flood events for the Pachang River, Taiwan. Water Resour. Manag. 19, 363–374. https://doi.org/10.1007/s11269-005-2073-2.
Ndehedehe, C.E., Anyah, R.O., Alsdorf, D., Agutu, N.O., Ferreira, V.G., 2019. Modelling the impacts of global multi-scale climatic drivers on hydro-climatic extremes (1901–2014) over the Congo basin. Sci. Total Environ. 651, 1569–1587. https://doi.org/10.1016/j.scitotenv.2018.09.203.
Ndehedehe, C.E., Agutu, N.O., 2022. Historical Changes in Rainfall Patterns over the Congo Basin and Impacts on Runoff (1903–2010), in: Congo Basin Hydrology, Climate, and Biogeochemistry. American Geophysical Union (AGU), pp. 145–163. https://doi.org/10.1002/9781119657002.ch9.
Nicholson, S.E., 2018. The ITCZ and the seasonal cycle over Equatorial Africa. Bull. Am. Meteorol. Soc. 99, 337–348. https://doi.org/10.1175/BAMS-D-16-0287.1.
Nicholson, S.E., Kim, J., Hoopingarner, J., 1988. Atlas of African rainfall and its interannual variability. Department of Meteorology, the Florida State University.
Nicholson, S.E., Fink, A.H., Funk, C., Klotter, D.A., Satheesh, A.R., 2022. Meteorological causes of the catastrophic rains of October/November 2019 in equatorial Africa. Glob. Planet. Change 208, 103687. https://doi.org/10.1016/j.gloplacha.2021.103687.
O'Loughlin, F.E., Neal, J., Schumann, G.J., Beighley, R.E., Bates, P.D., 2019. A LISFLOOD-FP hydraulic model of the middle reach of the Congo. J. Hydrol. https://doi.org/10.1016/j.jhydrol.2019.124203.
Paiva, R.C.D., Collischonn, W., Tucci, C.E.M., 2011. Large scale hydrologic and hydrodynamic modeling using limited data and a GIS based approach. J. Hydrol. 406, 170–181. https://doi.org/10.1016/j.jhydrol.2011.06.007.
de Paiva, R.C.D., Buarque, D.C., Collischonn, W., Bonnet, M.-P., Frappart, F., Calmant, S., Bulhões Mendes, C.A., 2013. Large-scale hydrologic and hydrodynamic modeling of the Amazon River basin. Water Resour. Res. 49, 1226–1243. https://doi.org/10.1002/wrcr.20067.
Paiva, R.C.D., Collischonn, W., Bonnet, M.-P., de Gonçalves, L.G.G., Calmant, S., Getirana, A., Santos da Silva, J., 2013. Assimilating in situ and radar altimetry data into a large-scale hydrologic-hydrodynamic model for streamflow forecast in the Amazon. Hydrol. Earth Syst. Sci. 17, 2929–2946. https://doi.org/10.5194/hess-17-2929-2013.
Papa, F., Prigent, C., Aires, F., Jimenez, C., Rossow, W.B., Matthews, E., 2010. Interannual variability of surface water extent at the global scale, 1993-2004. J. Geophys. Res. Atmospheres 115, 1–17. https://doi.org/10.1029/2009JD012674.
Paris, A., Calmant, S., Gosset, M., Fleischmann, A.S., Conchy, T.S.X., Garambois, P., Bricquet, J., Papa, F., Tshimanga, R.M., Guzanga, G.G., Siqueira, V.A., Tondo, B., Paiva, R., Silva, J.S., Laraque, A., 2022. Monitoring hydrological variables from remote sensing and modeling in the Congo River Basin. In: Tshimanga, R.M., N'kaya, G.D.M., Alsdorf, D. (Eds.), Geophysical Monograph Series. Wiley, pp. 339–366. https://doi.org/10.1002/9781119657002.ch18.
Pickands, J., 1975. Statistical inference using extreme order statistics. Ann. Stat. 3, 119–131.
Pontes, P.R.M., Fan, F.M., Fleischmann, A.S., de Paiva, R.C.D., Buarque, D.C., Siqueira, V.A., Jardim, P.F., Sorribas, M.V., Collischonn, W., 2017. MGB-IPH model for hydrological and hydraulic simulation of large floodplain river systems coupled with open source GIS. Environ. Model. Softw. 94, 1–20. https://doi.org/10.1016/j.envsoft.2017.03.029.
Prigent, C., Papa, F., Aires, F., Rossow, W.B., Matthews, E., 2007. Global inundation dynamics inferred from multiple satellite observations, 1993-2000. J. Geophys. Res. Atmospheres 112, 1993–2000. https://doi.org/10.1029/2006JD007847.

Revel, M., Ikeshima, D., Yamazaki, D., Kanae, S., 2019. A physically based empirical localization method for assimilating synthetic SWOT observations of a continental-scale river: A case study in the Congo basin. Water (Switz.) 11. https://doi.org/10.3390/w11040829.
Rodell, M., Famiglietti, J.S., 2002. The potential for satellite-based monitoring of groundwater storage changes using GRACE: The High Plains aquifer, Central US. J. Hydrol. 263, 245–256. https://doi.org/10.1016/S0022-1694(02)00060-4.
Saji, N.H., Goswami, B.N., Vinayachandran, P.N., Yamagata, T., 1999. A dipole mode in the tropical Indian Ocean. Nature 401, 360–363. https://doi.org/10.1038/43854.
Samba, G., Nganga, D., Mpounza, M., 2008. Rainfall and temperature variations over Congo-Brazzaville between 1950 and 1998. Theor. Appl. Clim. 91, 85–97. https://doi.org/10.1007/s00704-007-0298-0.
Scanlon, B.R., Zhang, Z., Save, H., Wiese, D.N., Landerer, F.W., Long, D., Longuevergne, L., Chen, J., 2016. Global evaluation of new GRACE mascon products for hydrologic applications. Water Resour. Res. 52, 9412–9429. https://doi.org/10.1002/2016WR019494.
Singh, V.P., 2018. Hydrologic modeling: progress and future directions. Geosci. Lett. 5, 15. https://doi.org/10.1186/s40562-018-0113-z.
Siqueira, V.A., Paiva, R.C.D., Fleischmann, A.S., Fan, F.M., Ruhoff, A.L., Pontes, P.R.M., Paris, A., Calmant, S., Collischonn, W., 2018. Toward continental hydrologic-hydrodynamic modeling in South America. Hydrol. Earth Syst. Sci. 22, 4815–4842. https://doi.org/10.5194/hess-22-4815-2018.
Sorí, R., Stojanovic, M., Nieto, R., Liberato, M.L.R., Gimeno, L., 2022. Spatiotemporal variability of droughts in the Congo River Basin: the role of atmospheric moisture transport. In: Tshimanga, R.M., N'kaya, G.D.M., Alsdorf, D. (Eds.), Geophysical Monograph Series. Wiley, pp. 187–203. https://doi.org/10.1002/9781119657002.ch11.
Sprintall, J., Cravatte, S., Dewitte, B., Du, Y., Gupta, A.S., 2020. ENSO oceanic teleconnections. In: El Niño Southern Oscillation in a Changing Climate, Geophysical Monograph Series, pp. 337–359. https://doi.org/10.1002/9781119548164.ch15.
Stein, K., Timmermann, A., Schneider, N., Jin, F.-F., Stuecker, M.F., 2014. ENSO seasonal synchronization theory. J. Clim. 27, 5285–5310. https://doi.org/10.1175/JCLI-D-13-00525.1.
Strassberg, G., Scanlon, B.R., Chambers, D., 2009. Evaluation of groundwater storage monitoring with the GRACE satellite: Case study of the High Plains aquifer, central United States. Water Resour. Res. 45, 1–10. https://doi.org/10.1029/2008WR006892.
Sun, L., Seidou, O., Nistor, I., Liu, K., 2016. Review of the Kalman-type hydrological data assimilation. Hydrol. Sci. J. 61, 2348–2366. https://doi.org/10.1080/02626667.2015.1127376.
Tabari, H., 2021. Extreme value analysis dilemma for climate change impact assessment on global flood and extreme precipitation. J. Hydrol. 593, 125932 https://doi.org/10.1016/j.jhydrol.2020.125932.
Tarek, M., Brissette, F.P., Arsenault, R., 2020. Evaluation of the ERA5 reanalysis as a potential reference dataset for hydrological modelling over North America. Hydrol. Earth Syst. Sci. 24, 2527–2544. https://doi.org/10.5194/hess-24-2527-2020.
Taschetto, A.S., Ummenhofer, C.C., Stuecker, M.F., Dommenget, D., Ashok, K., Rodrigues, R.R., Yeh, S.-W., 2020. ENSO Atmos. Teleconnections 309–335. https://doi.org/10.1002/9781119548164.ch14.
Tourian, M.J., Papa, F., Elmi, O., Sneeuw, N., Kitambo, B., Tshimanga, R.M., Paris, A., Calmant, S., 2023. Current availability and distribution of Congo Basin's freshwater resources. Commun. Earth Environ. 4, 174. https://doi.org/10.1038/s43247-023-00836-z.
Trenberth, K.E., 1997. The Definition of El Niño. Bull. Am. Meteorol. Soc. 78, 2771–2778. https://doi.org/10.1175/1520-0477(1997)078<2771:TDOENO>2.0.CO;2.
Tshimanga, R.M., Hughes, D.A., 2014. Basin-scale performance of a semidistributed rainfall-runoff model for hydrological predictions and water resources assessment of large rivers: The Congo River. Water Resour. Res. 50, 1174–1188. https://doi.org/10.1002/2013WR014310.
Tshimanga, R.M., Hughes, D.A., Kapangaziwiri, E., 2011. Initial calibration of a semi-distributed rainfall runoff model for the Congo River basin. Physics and Chemistry of the Earth, Parts A/B/C, 11th WaterNet/WARFSA/GWP-SA Symposium: IWRM for National and Regional Integration through Science, Policy and Practice 36, 761–774. https://doi.org/10.1016/j.pce.2011.07.045.
Tshimanga, R.M., N'kaya, G.D.M., Laraque, A., Nicholson, S.E., Onema, J.-M.K., Lumbuenamo, R., Alsdorf, D., 2022. Congo Basin Research, in: Congo Basin Hydrology, Climate, and Biogeochemistry. American Geophysical Union (AGU), pp. 1–11. https://doi.org/10.1002/9781119657002.ch1.
Vizy, E.K., Cook, K.H., 2012. Mid-twenty-first-century changes in extreme events over Northern and Tropical Africa. J. Clim. 25, 5748–5767. https://doi.org/10.1175/JCLI-D-11-00693.1.
Washington, R., Harrison, M., Conway, D., Black, E., Challinor, A., Grimes, D., Jones, R., Morse, A., Kay, G., Todd, M., 2006. African climate change: taking the shorter route. Bull. Am. Meteorol. Soc. 87, 1355–1366. https://doi.org/10.1175/BAMS-87-10-1355.
Washington, R., James, R., Pearce, H., Pokam, W.M., Moufouma-Okia, W., 2013. Congo Basin rainfall climatology: can we believe the climate models? Philos. Trans. R. Soc. B 368, 20120296. https://doi.org/10.1098/rstb.2012.0296.
Webster, P.J., Moore, A.M., Loschnigg, J.P., Leben, R.R., 1999. Coupled ocean–atmosphere dynamics in the Indian Ocean during 1997–98. Nature 401, 356–360. https://doi.org/10.1038/43848.
Wongchuig, S., Paiva, R., Espinoza, J.C., Collischonn, W., 2017. Multi-decadal Hydrological Retrospective: Case study of Amazon floods and droughts. J. Hydrol. 549, 667–684. https://doi.org/10.1016/j.jhydrol.2017.04.019.
Wongchuig, S., Cauduro Dias de Paiva, R., Biancamaria, S., Collischonn, W., 2020a. Assimilation of future SWOT-based river elevations, surface extent observations and discharge estimations into uncertain global hydrological models, 125473–125473 J. Hydrol. 590. https://doi.org/10.1016/j.jhydrol.2020.125473.
Wongchuig, S., Fleischmann, A., Paiva, R., Fadel, A., 2020b. Towards discharge estimation for water resources management with a semi-distributed model and local ensemble Kalman Filter data assimilation. J. Hydrol. Eng. https://doi.org/10.1061/(ASCE)HE.1943-5584.0002027.
Wongchuig, S.C., de Paiva, R.C.D., Siqueira, V., Collischonn, W., 2019. Hydrological reanalysis across the 20th century: A case study of the Amazon Basin. J. Hydrol. 570, 755–773. https://doi.org/10.1016/j.jhydrol.2019.01.025.
Wu, X., Okumura, Y.M., DiNezio, P.N., 2019. What controls the duration of El Niño and La Niña Events? J. Clim. 32, 5941–5965. https://doi.org/10.1175/JCLI-D-18-0681.1.
Yamazaki, D., Lee, H., Alsdorf, D.E., Dutra, E., Kim, H., Kanae, S., Oki, T., 2012. Analysis of the water level dynamics simulated by a global river model: a case study in the Amazon River. Water Resour. Res. 48, 1–15. https://doi.org/10.1029/2012WR011869.
Yuan, Y., Yang, S., Zhang, Z., 2012. Different Evolutions of the Philippine Sea Anticyclone between the Eastern and Central Pacific El Niño: possible Effects of Indian Ocean SST. J. Clim. 25, 7867–7883. https://doi.org/10.1175/JCLI-D-12-00004.1.
Zelazowski, P., Malhi, Y., Huntingford, C., Sitch, S., Fisher, J.B., 2011. Changes in the potential distribution of humid tropical forests on a warmer planet. Philos. Trans. R. Soc. A Math. Phys. Eng. Sci. 369, 137–160. https://doi.org/10.1098/rsta.2010.0238.
Zhou, C.R., Chen, Y.F., Huang, Q., Gu, S.H., 2017. Higher moments method for generalized Pareto distribution in flood frequency analysis. IOP Conf. Ser.: Earth Environ. Sci. 82, 012031. https://doi.org/10.1088/1755–1315/82/1/012031.
Zhou, L., Tian, Y., Myneni, R.B., Ciais, P., Saatchi, S., Liu, Y.Y., Piao, S., Chen, H., Vermote, E.F., Song, C., Hwang, T., 2014. Widespread decline of Congo rainforest greenness in the past decade. Nature 509, 86–90. https://doi.org/10.1038/nature13265.